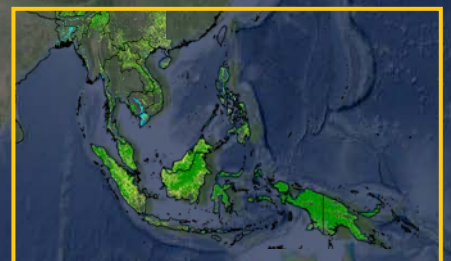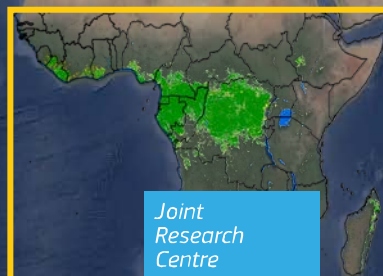# JRC TECHNICAL REPORT

Long-term monitoring of tropical moist forest extent (from 1990 to 2019)

Description of the dataset

Vancutsem C., Achard F., Pekel J.-F., Vieilledent G., Carboni S., Simonetti D., Marelli A., Gallego J.

2020

How to cite this report: Vancutsem C., Achard F., Pekel J.-F., Vieilledent G., Carboni S., Simonetti D., Marelli A., Gallego J , *Long-term monitoring of tropical moist forest extent (from 1990 to 2019),* EUR 30448 EN, Publications Office of the European Union, Luxembourg, 2020, ISBN 978-92-76-25320-4, doi:10.2760/70243, JRC122307.

Table of Contents

Acknowledgements

Authors

Christelle Vancutsem, Frédéric Achard, Jean-François Pekel, Ghislain Vieilledent, Silvia Carboni, Dario Simonetti, Andrea Marelli, Javier Gallego.

Joint
Research
Centre

Abstract

The need for accurate information on the state and evolution of tropical forest types at regional and continental scales is widely recognized, particularly to analyze the forest diversity and dynamics, to assess degradation and deforestation processes and to better manage these natural resources.

Here we document the approach that was developed by JRC to map and monitor the extent of moist tropical forests and their changes (degradation, deforestation and regrowth) over the last three decades (1990-2020) at fine spatial resolution (30 m × 30 m). The approach is based on the analysis of each valid observation from the Landsat archive and allows to capture disturbances with a short-duration appearance on satellite imagery such as selective logging, fires, and severe weather events (hurricanes, dryness).

This new approach allows characterizing the sequential dynamics of forest cover changes by providing transition stages from the initial observation period to the most recent year (2019 for this report). For the first time at the pantropical scale the occurrence and extent of forest degradation can be documented on an annual basis in addition to the monitoring of deforestation.

After a short introduction (chapter 1), this technical report describes the study area (chapter 2), the input data (chapter 3), the method that has been developed (chapter 4), and the outcomes of this study (chapter 5). A discussion is also provided regarding the specificities and added value of the outcomes (chapter 6), and the known limitations and future expected improvements (chapter 7).

This new pan-tropical scale deforestation and forest degradation monitoring system will contribute to the EU Observatory on deforestation, forest degradation, changes in the world's forest cover, and associated drivers, which is an action being implemented in the framework of the Communication from the Commission to step up EU action to protect and restore the World's forests (COM(2019) 352).

1 Introduction

Tropical moist forests (TMF) have a huge environmental value. They play an important role in biodiversity conservation, terrestrial carbon cycle, hydrological regimes, indigenous population subsistence and human health (**1-5**). They are increasingly recognized as an essential element of any strategy to mitigate climate change (**6, 7**). Deforestation, and degradation compromise the functioning of tropical forests as an ecosystem, lead to biodiversity loss (**1, 4, 5, 8, 9**) and reduced carbon storage capacity (**10-17**). Deforestation and fragmentation are increasing the risk of virus disease outbreaks (**18-20**).

For humanity wellbeing, sustainable economic growth and conservation of the remaining TMF constitute one of the largest challenges and shared responsibility. A consistent, accurate and geographically explicit characterization of the long-term disturbances at the pantropical scale is a prerequisite for elaborating a coherent territorial planning towards Sustainable Development Goals (SDGs) and the Nationally determined contributions (NDCs) of the Paris Agreement (2015). Advances in remote-sensing, cloud computing facilities, and free access to the Landsat satellite archive (**21-23**), enable systematic monitoring and consistent dynamic characterization of the entire TMF across a long period. Global maps have been derived to quantify tree cover loss since 2000 (**24-25**) and to identify remaining intact forest landscapes (**17**). However, detailed spatial information on the long-term dynamics of tropical moist forests and particularly on forest degradation and post-disturbances development stages is still missing to accurately estimate the carbon loss associated with forest disturbances (**2, 13, 15**) and assess their impact on biodiversity (**5, 8**).

Here we provide new information through a wall-to-wall mapping of tropical moist forest cover dynamics over a long-term period (January 1990 to December 2019) at 0.09 ha resolution (freely available from https://forobs.jrc.ec.europa.eu/TMF/). This validated dataset depicts the TMF extent and the related disturbances (deforestation and degradation), and post-disturbances recovery on an annual basis over the last three decades. A major innovation consists of characterizing the sequential dynamics of changes by providing transition stages from the initial observation period to the end of the year 2019, i.e. undisturbed forest, degraded forest, forest regrowth, deforested land, conversion to plantations, conversion to water, afforestation, and changes within the mangroves, as well as the timing (dates and duration), recurrence and intensity of each disturbance.

For the first time at the pantropical scale the occurrence and extent of the forest cover degradation is documented on an annual basis in addition to the deforestation. This has been achieved thanks to the analysis of each individual valid observation of the Landsat archive (see Data and Mapping method sections) allowing to capture short-duration disturbances such as selective logging, fires, and severe weather events (hurricanes, dryness). Deforestation in TMF cover is documented in an unprecedented comprehensive manner: (i) by covering a 30-year period of analysis, (ii) by mapping deforestation occurring after degradation and deforestation followed by a regrowth, (iii) by identifying specific forest conversion to commodities or water, (iv) by including changes within the mangroves, and (v) by documenting each deforestation event at the pixel level by its timing (date and duration), intensity, recurrence and when appropriate, start date and duration of post-disturbance regrowth.

The analysis of the yearly dynamics of TMF disturbances over the last 30 years underlines the importance of the degradation process in tropical moist forest ecosystems. The results of this analysis are presented in a peer-reviewed paper (**26**).

2   Study area and Forest types

Our study covers the tropical moist forest domain, which includes the following vegetation types (**27**): the lowland evergreen rain forest, the montane rain forest, the mangrove forest, the swamp forest, the tropical semi-evergreen rain forest, and the moist deciduous forest. Evergreenness varies from permanently evergreen to evergreen seasonal (mostly evergreen but with individual trees that may lose their leaves), semi-evergreen seasonal (up to about one third of the top canopy can be deciduous, though not necessarily leafless at the same time), and moist deciduous (dominant deciduous species with evergreen secondary canopy layer).

We do not intent to map specifically intact or primary forest as the Landsat observation period is too short to discriminate never-cut primary forest from second growth naturally recovered forest older than the observation period. However, by documenting all the disturbances observed over the last three decades, the remaining undisturbed TMF in 2019 is getting closer to the primary forest extent. Whereas our entire TMF - that includes undisturbed and degraded forests - in 1990 and 2019 are comparable, our undisturbed forest of 1990 and 2019 should be carefully compared.

Our study area covers the following Global Ecological Zones (**28**): 'Tropical rainforest', 'Tropical moist forest', 'Tropical mountain system' and 'Tropical dry forest' (**Figure 1**) and stops at the borders of China, Pakistan, Uruguay, and USA. The TMF are located mostly in the tropical moist and humid climatic domains but also include small areas of gallery forests in the tropical dry domain.

Figure 1. Extent of the study area.

The study area is defined using the ecological zones adopted by the FAO and includes the following zones: 'Tropical rainforest', 'Tropical moist forest', 'Tropical mountain system' and 'Tropical dry forest'.
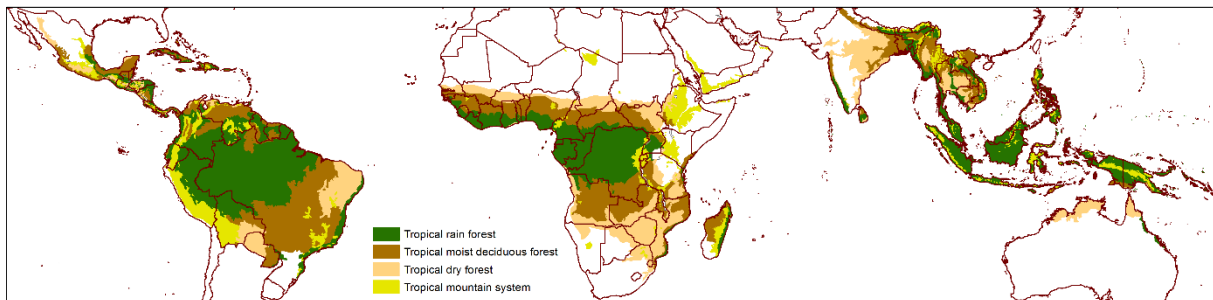
3 Data

The Landsat archive is the only free and long-term satellite image record suited for analysing vegetation dynamics at fine spatial resolution. We used the entire L1T archive (orthorectified top of atmosphere reflectance) acquired between July 1982 and December 2019 from the following Landsat sensors: Thematic Mapper (TM) onboard Landsat 4 and 5, Enhanced Thematic Mapper-plus (ETM+) onboard Landsat 7 and the Operational Land Imager (OLI) onboard Landsat 8 (**23, 29-31**). Landsat 4 was launched in July 1982 and collected images from its TM sensor until December 1993. Landsat 5 was launched in March 1984 and collected images until November 2011. Landsat 7 was launched in April 1999 and acquired images normally until May 2003 when the scan line corrector (SLC) failed (**32**). All Landsat 7 data acquired after the date of the SLC failure have been used in our analysis. Landsat 8 began operational imaging in April 2013.

The Landsat archive coverage presents large geographical and temporal unevenness (**29, 33**). The main reason for the limited availability of images for some regions is that Landsat 4 and 5 had no onboard data recorders, and links with data relay satellites failed over time; cover was therefore often limited to the line of sight of receiving stations (**31**). Commercial management of the programme from 1985 to the early 1990s led to data acquisitions being acquired mostly when pre-ordered (**29**). From 1999 onwards, the launch of Landsat 7 and its onboard data recording capabilities, associated with the continuation of the Landsat 5 acquisitions, considerably improved global coverage.

In the tropical regions, Africa is particularly affected by the limited availability of image acquisitions, especially in the first part of the archive. From a total of around 1 370 860 Landsat scenes that were available for our study area, only 265 098 scenes were located in Africa (in comparison, 573 589 and 532 173 scenes were respectively available in South America and Asia). The most critical area is located around the Gulf of Guinea, with an overall average number of valid observations (i.e. without clouds, hazes, sensor artefacts and geo-location issues) over the full archive (**Figure 2**) of fewer than 50 per location (pixel) and with the first valid observations starting mostly at the end of the 1990s (**Figure 3**). Small parts of Ecuador, Colombia, Salomon Islands and Papua New Guinea present a similar low number of total valid observations, often with an earlier first valid observation around the end of the 1980s. Apart from these regions, the first valid observation occurs mostly within periods 1982-1984, 1984-1986, or 1986-1988 for Latin America, Africa and Southeast Asia, respectively.

Figure 2. Total number of valid observations per pixel from the full Landsat archive (1982-2019) over the pan-tropical belt.
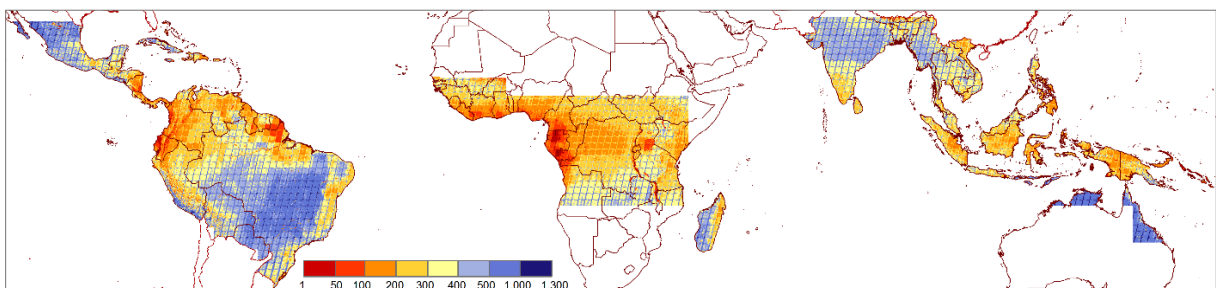
Figure 3. Year of first valid observation from the full Landsat archive (1982-2019), across the pan-tropical belt.
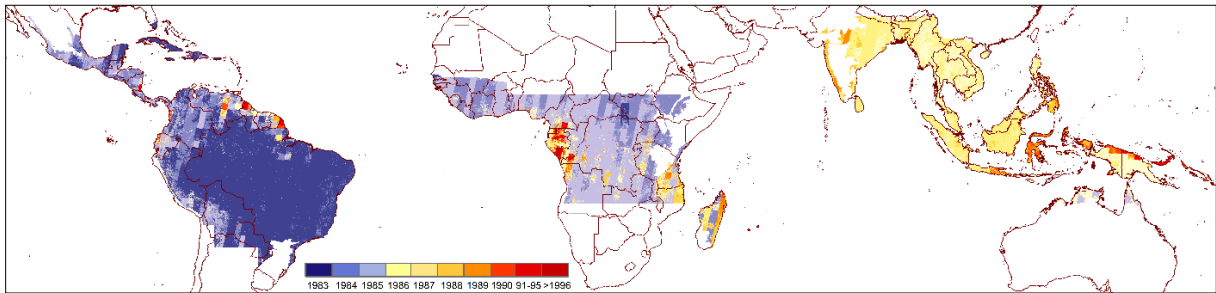
The average number of annual valid observations (**Figure 4**) shows a stepped increase during the 38-year period for the three continents, with two major jumps: in 1999 with the launch of Landsat 7, and in 2013 with the launch of Landsat 8. There is also a clear drop in 2012 for Southeast Asia and Latin America with the decommissioning of Landsat 5 in November 2011, and a small drop in 2003 as a consequence of the Landsat 7 SLC off issue. There are major differences between Africa and the two other continents: Africa has significantly fewer valid observations, in particular during the period 1982-1999, and a much larger increase in number of observations from 2013.

Figure 4. Annual average number of valid observations per pixel (by continent) over the period 1982-2019 Landsat archive for the tropical moist forest domain.
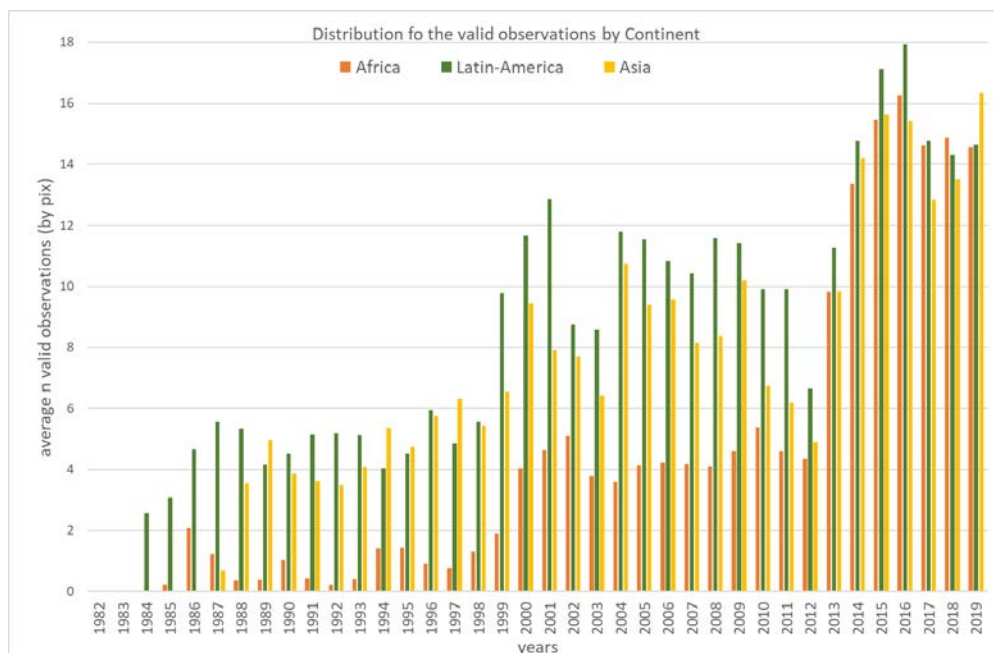
The geographical unevenness of the first year of acquisition constrains the monitoring capability period. Our method accounts for this constraint notably by recording the effective duration of the archive at the pixel level (see next section on the mapping method).

Data quality issues affecting the Landsat collection were addressed by excluding pixels where (i) detector artefacts occur (manifested as random speckle or striping), (ii) one or

more spectral bands are missing (typically occurring at image edges) or (iii) scene geo-location is inaccurate.

4 Method

4.1 Mapping method

In order to map the area dynamics (extent and changes) of the TMF over a long period, we developed an expert system that exploits the multispectral and multitemporal attributes of the Landsat archive to identify the main change trajectories over the last 3 decades and uses ancillary information to identify sub-classes of forest conversion (**Annex 1**). The inference engine of our system is a procedural sequential decision tree, where the expert knowledge is represented in the form of rules. Techniques for big data exploration and information extraction, namely visual analytics (**34**) and evidential reasoning (**35**), were used similarly to a recent study dedicated to global surface water mapping (**33**). The advantages of these techniques for remotely sensed data analysis are presented in this previous study (**33**), notably for accounting for uncertainty in data, guiding and informing the expert's decisions, and incorporating image interpretation expertise and multiple data sources. The expert system was developed and operated in the Google Earth Engine (GEE) geospatial cloud computing platform (**22**).

The mapping method includes four main steps (**Figure 5**) described hereafter: (i) single-date multi-spectral classification into three classes, (ii) analysis of trajectory of changes using the temporal information and production of a 'transition' map (with seven classes), (iii) identification of sub-classes of transition based on ancillary datasets (**Annex 1**) and visual interpretation, (iv) production of annual change maps.

Figure 5. Main steps of the mapping method
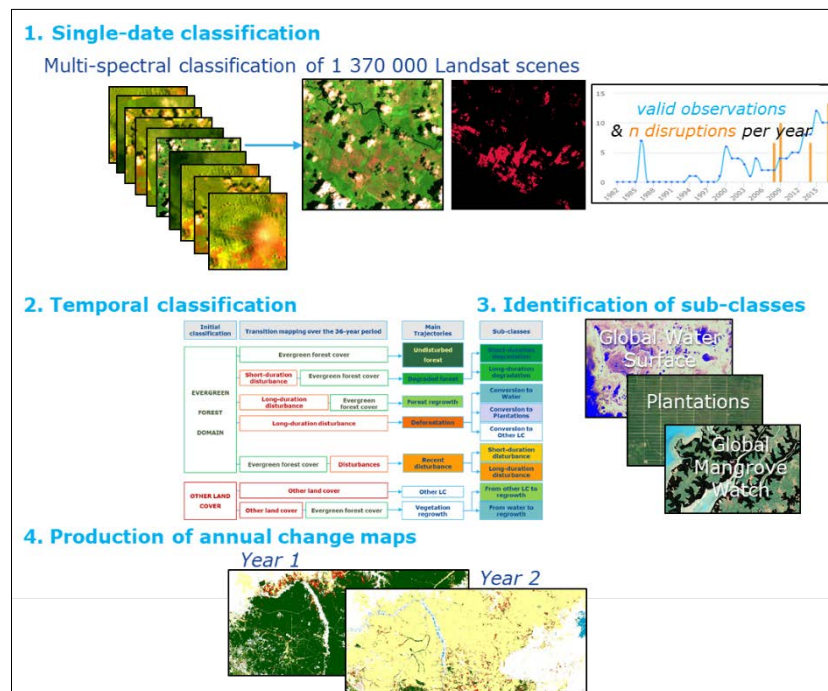
4.1.1 Single-date multi-spectral classification

In the first step, each image of the Landsat archive was analysed on a single-date basis (through a multi-spectral classification), whereas previous large-scale studies used annual syntheses or intra-annual statistics such as the mean and standard deviation of available Landsat observations (**36-42**). Classification of individual images is challenging but

presents three main advantages: it allows (i) to capture the disturbance events that are visible only over a short period from space, such as logging activities, (ii) to record the precise timing of the disturbances and the number of *disruption observations,* and (iii) to detect the disturbance at an early stage, i.e. even if the disturbance is starting at the end of the year, it is detected and counted as a disturbance for this year whereas other approaches notably based on composites will detect the disturbance with a delay of one year.

A *disruption observation* is defined here as an absence of tree foliage cover within a 0.09 ha size Landsat pixel. The number of *disruption observations* constitutes a proxy of disturbance intensity.

Each pixel within a Landsat image was initially assigned through single-date multi-spectral classification to one of three following classes: (i) *potential moist forest cover*, (ii) *potential disruption*, and (iii) *invalid observation* (cloud, cloud shadow, haze and sensor issue).

Multispectral clusters were defined first by establishing a spectral library capturing the spectral signatures of the land cover types and atmosphere perturbations that are present over the pan-tropical belt and targeted for these three classes : (i) moist forest types, (ii) deciduous forest, logged areas, savannah, bare soil, irrigated and non-irrigated cropland, evergreen shrubland and water (for the *potential disruption* class) and (iii) clouds, haze, cloud shadows (for the *invalid observations*). A total sample of 38 326 sampled pixels belonging to 1 512 Landsat scenes (L5, L7 and L8), were labelled through visual interpretation. The HSV (*hue, saturation, value*) transformation of the spectral bands - well adapted for satellite image analysis (**33**, **43**) - were used to complement the spectral library. These components were computed using a standard transformation (52) for the following Landsat band combination: short-wave infrared (SWIR2), near infrared (NIR) and red. The stability of *hue* to the impacts of atmospheric effect is particularly desirable for identifying *potential disruption* in the humid tropics. The sensitivity of *saturation* and *value* to atmospheric variability is mainly used to detect *invalid* observations (haze). *Value* is particularly useful for identifying cloud shadows. The thermal infrared band (TIR) was relevant to detect *invalid* observations (clouds, haze) and bare soil, and the Normalized Difference Water Index (NDWI) to identify irrigated areas. The information held in the spectral library was analyzed through visual analytics to extract equations describing class cluster hulls in the multidimensional feature-space (**Figure 6**). An exploratory data analysis tool designed in a previous study (**33**) was used to support the interactive analysis.

4.1.2   Transition classes

The temporal sequence of classes (i) and (ii) was used to determine the seven transition classes, Evidential reasoning was used to guide class assignment by taking into consideration the temporal trajectory of single-date classifications, as spectral overlap between land cover types may occur only at specific periods of the year. For instance, pixels covered by deciduous forests, grassland or agriculture, may behave – from a spectral point of view – as *potential moist forest cover* during the humid seasons and as *potential disruptions* during the dry seasons, and, consequently, can be assigned to the *other land cover* transition class. Disturbed moist forests (degraded or deforested) are appearing as *potential moist forest cover* at the start of the archive and as *potential disruption* assignments later.

The temporal sequence of single-date classifications at pixel scale was analysed to first determine the initial extent of the TMF domain and then to identify the change trajectories from this initial forest extent (**Figure 7**).

Figure 6. Multispectral feature space
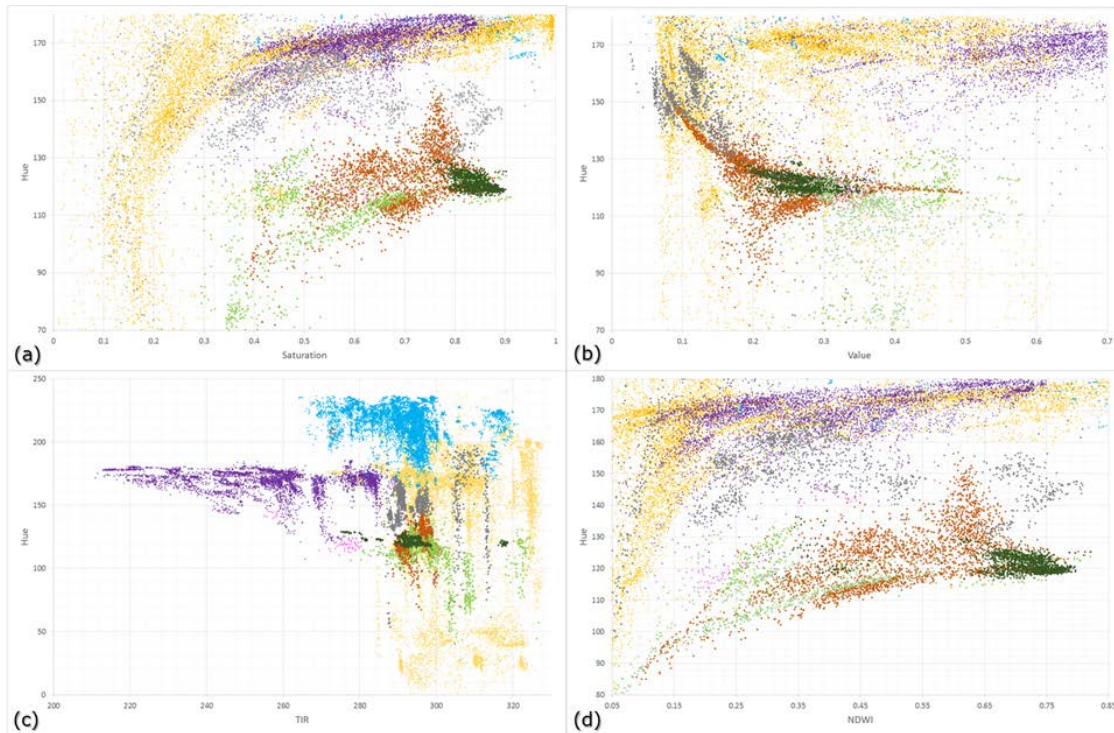
The Multispectral feature space inlcudes the following clusters: moist forest (dark green points), non-evergreen cover (orange for bare soils, brown for deciduous vegetation, light green for agriculture, blue for water) and invalid pixels (grey for shadows, purple for clouds and pink for haze): (a) hue versus saturation (both from SWIR2, NIR, red), (b) hue versus value (both from SWIR2, NIR, red), (c) hue (from SWIR2, NIR, red) versus TIR, (d) hue versus NDWI.

Figure 7. Methodological steps for the definition of the transition classes.
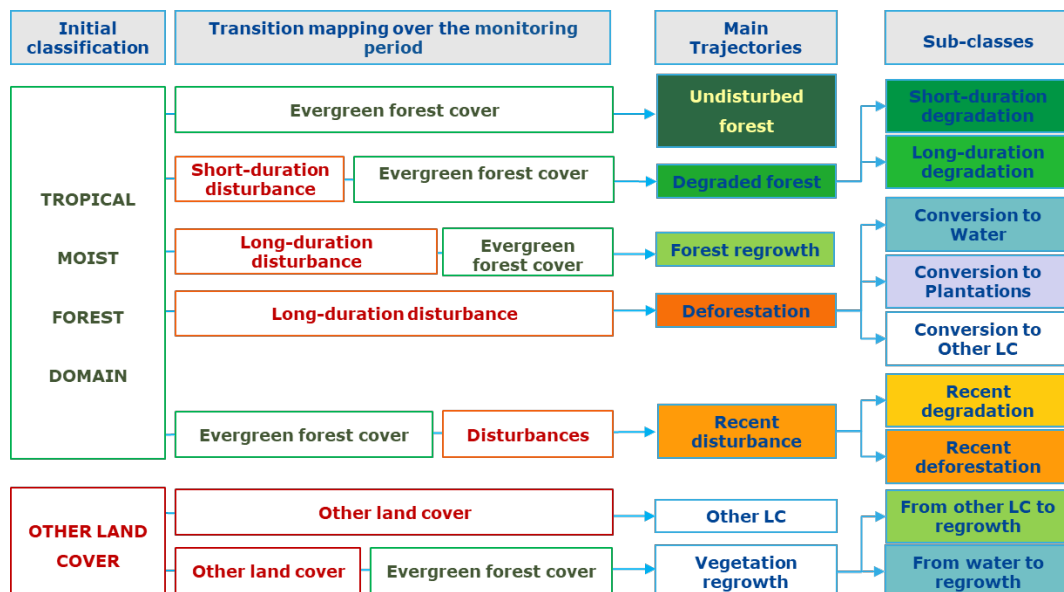
Long-term changes cannot be determined uniformly for the entire pan-tropical region because the observation record varies (see **Data**), e.g. the first year of observation (**Figure 8**) is c. 1982 for Brazil and c. 2000 along the Gulf of Guinea. We have addressed this geographic and temporal discontinuities of the Landsat archive by determining at the pixel level (i) a reference initial period (baseline) for mapping the initial TMF extent and (ii) a monitoring period for detecting the changes. The data gaps at the beginning of the archive were tackled by requiring a minimum period of four years with a minimum of three valid observations per year or a minimum of five years with two valid observations per year from the first available valid observation. Hence, lower is the annual number of valid observations, higher is the length of the initial period. This minimizes the risk of inclusion of non-forest cover types (such as agriculture) and deciduous forests in the baseline when there are few valid observations over a short period. In addition, we have reduced the commission errors in our baseline by accounting for possible confounding with commodities, wetlands, bamboo, and deciduous forest (**Annexes 1 and 2**).

Figure 8. First year of the monitoring period used for changes analysis.
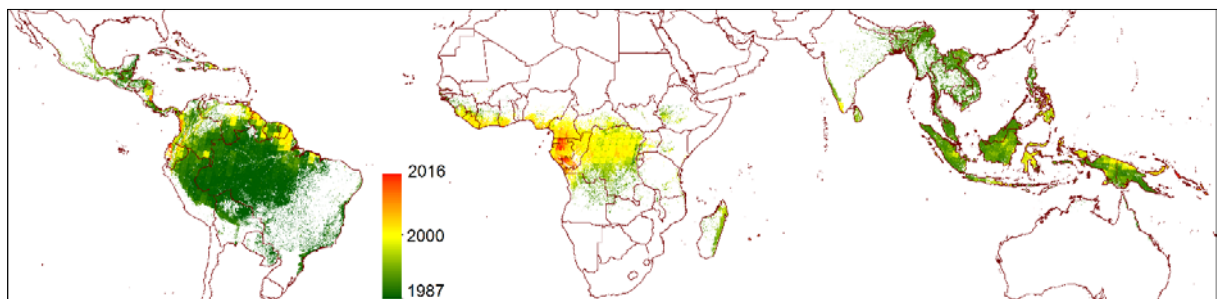
From our initial TMF extent, we identified seven main transition classes (**Figure 7**) which are defined thereafter. The first year of the monitoring period (that follows the initial period) is represented at figure 8; it starts at the earliest in year 1987 (mostly for South-America) and, for very limited cases, at the latest in 2016 (e.g. Gabon).

Although no ecosystem may be considered truly undisturbed, because some degree of human impact is present everywhere (**44**), we define the undisturbed moist forests (class 1) as tropical moist (evergreen or semi-evergreen) forest coverage without any disturbance (degradation or deforestation) observed over the Landsat historical record (see **Data**). Our TMF baseline may include old forest regrowth (old secondary forests) or previously degraded forests forest as the Landsat observation period is too short to discriminate never-cut primary forest from second growth naturally recovered forest older than the observation period. This class includes two sub-classes of bamboo-dominated forest (class 1a) and undisturbed mangrove (class 1b).

A *deforested land* (class 2) is defined as a permanent conversion from moist forest cover to another land cover whereas a *degraded forest* (class 3) is defined as a moist forest cover where disturbances were observed over a short time period. Here we assumed that the duration of the disturbance (and consequently the period over which we detect the disturbance with satellite imagery) is a proxy of the disturbance impact, i.e. higher is the duration of the detected disturbance, higher is the impact on the forest, and higher is the risk to have a permanent conversion of the TMF. By considering short-term disturbances we include logging activities, fires and natural damaging events such as wind breaks and extreme dryness periods. Hence, we are getting closer to the most commonly accepted definition of the degradation (**45**) that considers a loss of productivity, a loss of

biodiversity, unusual disturbances (droughts, blowdown), and a reduction of carbon storage.

The threshold applied on the duration parameter used to separate *degraded forests* from *deforested land* is based on our knowledge of the impacts of human activities and of natural or human-induced events such as fires. We identified empirically two levels of degradation: (class 3a) degradation with short-duration impacts (observed within a 1-year maximum duration), which includes the majority of logging activities, natural events and light fires, and (class 3b) degradation with long-duration impacts (between one and 2.5 years) which mainly corresponds to strong fires (burned forests). Most of the degradation (63.5%) are observed over less than six-month durations (**Figure 9**). All disturbance events for which the impacts were observed over more than 2.5 years (900 days) were considered as deforestation processes, with 86% of such deforestation events observed over more than five years. When a deforestation process is not followed by a regrowth period at least over the last 3 years, it is considered as a *Deforested land*. Deforested land are also characterized by the recurrence of disruptions, i.e. the ratio between the number of years with at least one disruption observation and the total number of years between the first and last disruption observations. This information allowed to discriminate deforestation without prior degradation from deforestation occurring after degradation, the second one having a lower recurrence due to the period without any disruption between the degradation and deforestation phases.

For the recent degradation and deforestation (class 4) that initiated in the last three years (after year 2016) and that cannot yet be attributed to a long-term conversion to a non-forest cover, owing to the limited historical period of observation, specific rules were applied. Within this class, we separated degradation from deforestation, by taking a duration of minimum 366 days for the years 2017-2018 and a threshold of 10 disruptions for the last year (2019) to consider a *deforested land*.

Figure 9. Distribution of the duration of disturbances recorded over the period 1990-2016 for each continent.
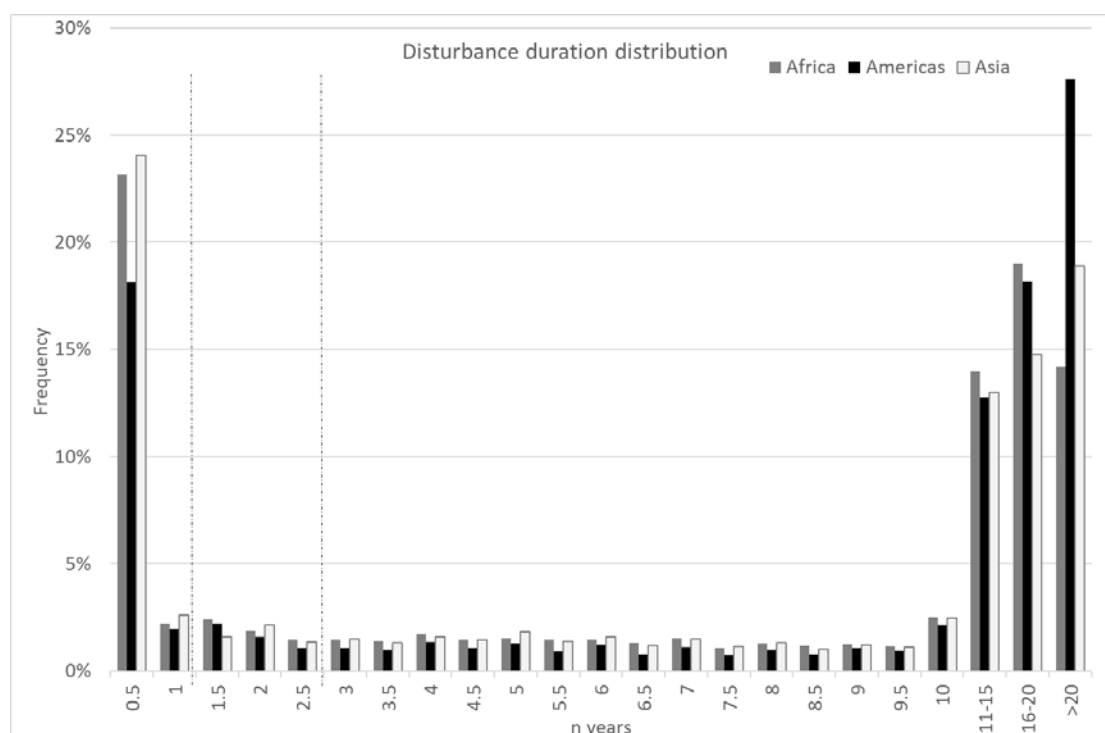
The temporal thresholds used to define short-duration degradation, long-duration degradation and deforestation are represented as dashed lines (at 1 and 2.5 years, respectively).Two third of the degradation disturbances are observed during the first 6 months. Most of the deforestation disturbances (86%) are observed over more than five years duration.

A *forest regrowth* (class 5) is a two-phase transition from moist forest to (i) deforested land and then (ii) vegetative regrowth. A minimum 3-years duration of permanent moist forest cover presence is needed to classify a pixel as forest regrowth (to avoid confusion with agriculture).
The *other land cover* (class 6) includes savannah, deciduous forest, agriculture, evergreen shrubland and non-vegetated cover.
Finally, the *Vegetation regrowth (class 7)* consists of a transition from other land cover to vegetation regrowth and includes two sub-classes of vegetation regrowth according to the age of regrowth (between 3 and 10 years, and between 10 and 20 years) and a transition class from water to vegetation regrowth.

4.1.3   Identification of sub-classes

The third mapping step allowed to identify three sub-classes from the *deforested land* class. We geographically assigned deforestation to the conversion from TMF to tree plantations - mainly oil palm and rubber (class 2a), water surface (discriminating permanent and seasonal water)- mainly due to new dams (class 2b), and other land cover - agriculture, infrastructures, etc. (class 2c) using ancillary spatial datasets completed by visual interpretation of high-resolution (HR) imagery (**Annex 1**). Finally, we have re-assigned disturbances when detected within two geographically specific tropical forest formations: (i) the bamboo dominated forest, and (ii) the semi-deciduous transition tropical forest (**Annex 2**).

Each disturbed pixel (degraded forest, deforested land, or forest regrowth) is characterized by the timing and intensity of the observed disruption events. The start and end dates of the disturbance allows identifying in particular the timing of creation of new roads or of logging activities and the age of forest regrowth or degraded forests. Three decadal periods have been used in the transition map to identify age sub-classes of degradation and forest regrowth: (i) before 2000, (ii) within 2000-2009 and (iii) within 2010-2019. The number of annual disruption observations combined with the duration, can be used as a proxy for the disturbance intensity and impact level.

4.1.4   Annual change dataset

In the last mapping step, we created a collection of 30 maps providing the spatial extent of the TMF and disturbance classes on a yearly basis, from 1990 to 2019, using dedicated decision rules.

To obtain the annual classes, we combined the transition map with the following spatial layers: (i) number of disruption observations per year, (ii) first and last year of a disturbance period (YearMin and YearMax), (iii) recurrence of disruption observations (iv) Start Year of the archive (first year after the initial period), and (v) number of valid observations per year. The creation of annual maps is made from the following rules (where $Year_i$ stands for year 1990 to 2019):

    a) Deforestation that occurs after degradation is separated from direct deforestation using the recurrence value. The starting years of the disturbances (two in the case of a degradation before deforestation) are recorded (YearMin and YearMin2, respectively).

b) A disturbance is classified as new disturbance in YearMin (for degradation or direct deforestation) or YearMin2 (for deforestation after degradation).

c) A disturbance is classified as ongoing disturbance after YearMin or YearMin2 until YearMax.

d) In the case of a degradation disturbance, a pixel is classified as degraded forest after YearMax.

e) A disturbed pixel of the TMF domain is characterized into one of the three following timing periods: (i) when $Year_i$ is before StartYear, (ii) when $Year_i$ is after the StartYear and the pixel is within tree plantation areas, (ii) when $Year_i$ is after the StartYear and the pixel is outside tree plantation areas.

f) In the case of a deforestation disturbance, a pixel is classified as new regrowth on YearMax + 1, and then as ongoing regrowth from YearMax + 2.

g) A pixel is classified as permanent water or as seasonal water if located within the permanent water area or within the seasonal water area in the GWS annual dataset, respectively.

h) A pixel is classified as other land cover for $Year_i$ if located outside the moist forest domain and with at least one valid observation available during $Year_i$.

i) A pixel is classified as no data for $Year_i$ if no valid observations are available for $Year_i$.

In order to discriminate deforestation without prior degradation from deforestation occurring after degradation, we applied two conditions to consider that deforestation occurred after degradation: (i) a recurrence value lower than 58%, or (ii) a recurrence value lower than 70% with at least 6 years without any disruption events between the degradation and the deforestation disturbances. These conditions were determined empirically by analyzing various sequences of logged and deforested areas.

In the case of a degradation not followed by a deforestation, two temporal sequences can be potentially observed: (a) only one degradation disturbance is observed with less than 3 years duration and no other disruption events are detected until the end of the observation period, or (b) two degradation disturbances are observed and are separated by a break of a minimum 4 years period without disruption events.

4.2 Validation

The validation approach includes three steps to produce an accuracy assessment: (i) the sampling design, (ii) the response design and (iii) the production of confusion matrices and estimates of uncertainties. The sampling design consisted of defining the spatial distribution of the sample within our study zone. The response design consisted of defining the protocol of measurements over the sample plots, including the selection of the dates of Landsat images to be interpreted.

4.2.1 Sampling design

The most frequent sampling approach for validating land cover maps is a stratified random sampling with strata defined from the classes of the map to be validated and with an independent random sample in each stratum (**46-48**). However, in our case, the transition map depicted temporal land cover changes that made this solution difficult to apply. Here we selected a stratified systematic sampling scheme, which provides unbiased estimators of accuracy, although it leads to a non-unbiased and more complex estimation of the variances. The main considerations for this choice are:

• Under spatial correlation decreasing with the distance, systematic sampling is more accurate than random sampling, i.e. the actual sampling variance is lower. However, there is no unbiased estimator for the variance of systematic sampling and the usual random sampling estimator overestimates the systematic sampling variance, leading to a conservative accuracy assessment (**49-50**).

• If the sample size or the stratification are modified after the plot data collection start (e.g. because of changes in resources or improvement of the stratification), traditional systematic sampling with independent sampling may lead to a completely new sample (**50**). Our selected stratified systematic sampling minimized this drawback by using a common pattern of ranked replicates for all strata.

• Bi-dimensional systematic sampling usually relies on a regular grid, which should be applied in principle on an equal-area projection. Although geographical coordinates do not correspond to an exact equal-area projection, the area distortion of geographical coordinates has a limited impact in tropical regions.

The sample was designed using three steps: (i) the preparation of a two-level systematic grid of potential sample points, (ii) the creation of a stratification layer by combining the transition map with an ancillary layer and (iii) the selection of a set of second-level replicates to reach the target number of sample plots per stratum and continent.

We first defined a grid of regular blocks of 1° × 1° latitude–longitude size that covered our study zone. A random location was selected within one block, then the set of points that occupied the same position in each block defined replicate). The location of the second replicate was selected randomly within the 1° × 1° block among the locations that maximized the distance from replicate 1. The distance $d(1,2)$ between replicate 1 and 2 was the minimum distance between two points from each replicate that could belong to adjacent sampling blocks. For squared sampling blocks, there was only one location that reached the maximum distance for replicate 2. Replicates 1 and 2 constituted together a new systematic pattern following diagonal lines. Additional replicates could be added to intensify the sampling. To preserve a spatial distribution that was as homogeneous as possible, the location of each additional replicate was selected at random among those that maximized the distance to the previously selected replicates. Under the assumption that spatial correlation is higher at short distances, by maximising the distance between replicates, we reduced the redundancy of the information provided by the sample (**50**). The use of 1° × 1° blocks implies that the block size diminishes when moving away from the equator. Although this effect is limited within the tropics, we handled it by reducing

the number of plots along each geographical parallel through fraction downgrading between replicates[66]. The parallel at latitude a has a relative length of approximately $\cos(a)$ compared with the equator. Therefore, a portion of $[1 - \cos(a)]$ plots belonging to replicate 1 was downgraded to replicate 2, a portion of $[2 \times (1 - \cos(a))]$ was downgraded from replicate 2 to 3, and so on.

**Figure 10**. Example of systematic blocks of 1° by 1° longitude–latitude
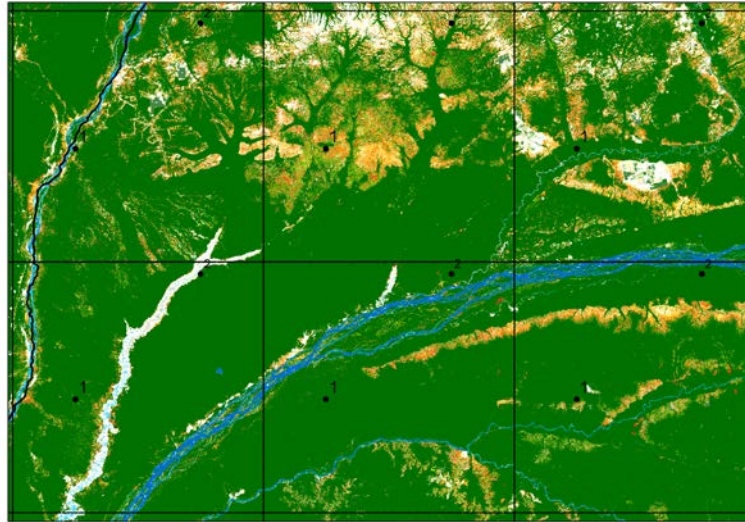
The figure is located over an area in the Democratic Republic of the Congo (around 350 km × 250 km in size and centred on 19.5°E, 2°N) with the transition layer in the background and shows replicates 1 and 2 (one replicate is the set of points that occupy the same position in each block),.

In the second step, we used the main classes of the transition map as core layers for the stratification, i.e. undisturbed, degraded forest, forest regrowth, deforested land, recent disturbances and other land cover. Moreover, in order to better assess potential omission errors in the mapping of disturbances, we added a supplementary (sub)stratum within the *undisturbed forest* stratum using the GFC dataset (**24**) as an ancillary spatial layer. To compensate for the shorter time coverage of the GFC dataset (compared with our dataset) we enlarged the GFC loss areas using a spatial buffer of 5 km. This was intended as a proxy for GFC past deforestation (i.e. before 2000), as new deforestation often occurs close to places where deforestation has occurred in the past. This led to the division of the undisturbed forest stratum into two strata: stratum 1 (undisturbed forest outside the GFC loss buffer) and stratum 2 (undisturbed forest within the GFC loss buffer). Overall, this resulted in a total of seven strata (

Figure 11).

Figure 11. Validation response design: process of selection of dates of Landsat images within the seven strata and three periods, to be interpreted in the reference validation dataset.
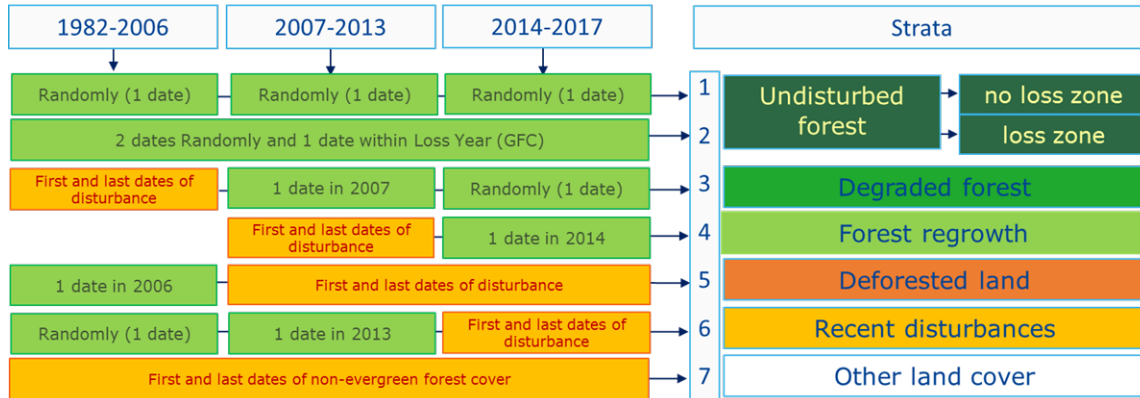
Regarding the availability of information on the structure of the variance of the target variables across the strata, there is a variety of criteria that can be used to optimize the sampling allocation, for example the traditional Neyman's rule (**51**) or multivariate algorithms (**52**). As we were missing such knowledge on the variability of target variables per stratum, we allocated the same sample size (250 sample plots) to each stratum and each continent, leading to heterogeneous numbers of plots per replicate, stratum and continent. For example, for the large stratum 7 in Africa, all 197 sample plots from replicate 1 were allocated and 53 sample plots in replicate 2 were selected randomly to meet the target of 250 plots. For a smaller-sized stratum, higher-ranked replicates needed to be considered in order to find 250 plots (e.g. up to replicate 8 for stratum 2 in Africa). In spite of this sampling heterogeneity, the sampling algorithm ensured spatial regularity and avoided pairs of sample plots that were very close to each other. The overall sample consisted of 1 750 sample plots by continent (7 strata × 250 plots), i.e. 5 250 sample plots for the overall study area (**Figure 12**).

Figure 12. Sampling plots (5250) used for the validation and accuracy assessment.
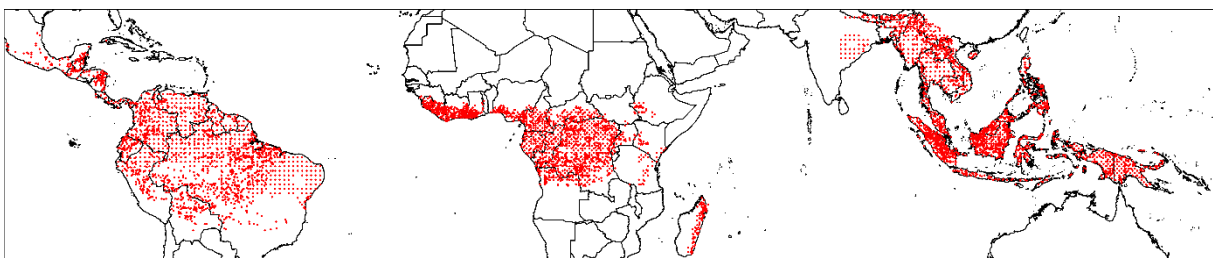
4.2.2 Response design

The reference dataset of land cover classes was created through visual expert interpretation of Landsat images at several dates and of recent higher resolution satellite images when available.

Each reference sample plot was assessed over a box size of 3 × 3 Landsat pixels centered on one of the 5 250 sample points. For each sample plot, a sub-set of Landsat images was selected for visual interpretation. For each image and sample plot (0.81 ha size), the interpreter selected one of the following land cover labels: (i) *forest cover*, (ii) *mostly non-forest*, (iii) *minor non-forest*, or (iv) *invalid*. A *forest cover* label corresponds to mature trees or vegetation regrowth (mosaic of shrubs and trees), covering the full plot (9 pixels).

The *mostly non-forest* label corresponds to a sample plot including at least five pixels with a *non-forest cover* (including disruption observations and other non-evergreen forest cover such as savanna, agriculture, and water surface). The interpreter assigned a *minor non-forest* label to the sample plot when one to four Landsat pixels with *non-forest* spectral signature were observed.

As it was not possible to interpret all the Landsat images available for each sample plot, we selected a subset of Landsat image dates for the visual interpretation, with the aim of optimizing the assessment of commission and omission errors and the resulting uncertainties (**Figure 11**), as follows:

- The Landsat images were selected from the full archive with at least one image within each of three key periods: (i) very recent years (2014-2017) corresponding to the acquisition period of Landsat 8 data, (ii) recent years (2007-2013) and (iii) historical period (before 2007).

- To assess the commission errors, we validated the detection of *disruption observations* from the same Landsat image that led to its detection. For each sample plot belonging to a disturbed stratum (i.e. strata 3-6) or to the *other land cover* stratum, the Landsat images corresponding to the dates of first and last *disruption observations* (or the dates of the non-evergreen forest cover observations for strata 7) were selected for visual interpretation.

- To assess omission errors (i.e. potential missed *disruption observations*), we validated the periods without *disruption observations* (green boxes in

Figure 11) as follows. For stratum 1 (undisturbed forest with no GFC loss), three dates from the series of existing Landsat images were selected randomly, one for each of the three periods. For stratum 2 (undisturbed forest within the GFC loss buffer), three dates from the series of existing Landsat images were selected for visual interpretation: one date selected during the GFC loss year when the sample plot was covered by GFC loss pixels and two dates were selected randomly from Landsat images available during the two remaining periods. For strata 3-6, one date was selected randomly from available Landsat images during each forest/regrowth period (periods without *disruption observations*). In these cases (strata 3-6), the year just after or just before a period with *disruption observations* was preferentially selected in order to validate the duration of the disturbance period; for example, for stratum 3 an image from 2007 was selected instead of a random selection from the period 2007-2013 (as the last disruption was observed before 2007).

This process of selection of Landsat images led to the selection of two to four images per sample plot and resulted in a total of 14 295 Landsat images to be visually interpreted.

4.2.3   Interpretation interface/tool

To interpret satellite images over the sample plots, a GEE web interface was developed to facilitate the photo-interpretation task by displaying (i) Landsat images at specific dates (see the subsection 'Response design' above), (ii) high-resolution (HR) images from the Digital Globe or Bing collections, and (iii) the sample box for each image.

For each sample plot and for each Landsat image, the expert validator had to select one class from the four land cover classes defined in the response design phase (*forest cover*, mostly *non-forest cover*, *minor non-forest cover*, or *invalid*). The expert validator did not have access to the results of our mapping approach (transition map or single-date classification) to avoid potential bias during this interpretation phase.

When an HR image was available, a more detailed land cover legend was used with the following classes: (i) *dense forest* (continuous tree cover with > 90% crown cover); (ii) *open forest* (non-continuous tree cover with > 50% crown cover); (iii) mostly *shrubland*; (iv) *forest/shrubland mosaic* (at least 10% of shrubs); (v) *minor non-forest* (10-50% non-forest cover); (vi) *mostly non-forest* (at least 50% non-forest cover); or (vii) *invalid* (no HR image available or clouds). Unfortunately, the exact dates of HR images are not usually available from GEE. Therefore, the HR interpretations were used in combination with the Landsat interpretations: (i) to support evidence in the validation process of the single-date classification algorithm, and (ii) to assess the accuracy of the transition classes and uncertainties of area estimates.

4.2.4   Accuracy assessment of the single-date classification algorithm

Our reference sample dataset was first used to assess the performance of the single-date classification algorithm in terms of errors of omission and commission. The accuracy was measured against the Landsat interpretations of the reference sample. The HR interpretations are provided in the detailed confusion matrix as complementary information to enable a better understanding of the commission and omission errors.

The HR interpretations were reclassified into five larger classes to make them comparable with the legend of the Landsat and single-date interpretations: (i) *forest*, (ii) *mostly non-forest*, (iii) *minor non-forest*, (iv) *shrub*, and (v) *invalid*. The *minor non-forest* and the *open forest* labels were grouped in one class (iii). The *mostly shrubland* and the *forest/shrubland mosaic* were grouped in one class (iv).

Using the full reference sample, a confusion matrix between the Landsat-based visual interpretations and the class values of our transition map was produced (for the three classes *forest cover*, *mostly non-forest*, and *minor non-forest)* from which a simplified 2-classes confusion matrix was derived with the forest and non-forest (including *mostly non-*

23

forest and *minor non-forest*) classes. This was used to estimate overall accuracy and related omission and commission errors.

As the single-date classification was done using different sensors (TM, ETM+ and OLI sensors) onboard different satellites, we verified the consistency of classifier performance across the main sensors (L5, L7 and L8) by estimating the omission and commission errors for each sensor. Finally, the validation results were analysed by continent and for the different land cover strata, as well as for different disturbance intensities.

4.2.5 Accuracy assessment of the transition map and uncertainties of area estimates

Our reference dataset of sample plots was then used for the accuracy assessment of the transition map and for estimating errors in area estimates. For this accuracy assessment exercise, we considered the land cover classes of the transition map to produce four new classes at the scale of the sample plots (3 × 3 pixels) in order to make them comparable with the reference dataset: (i) *fully undisturbed forest* (all nine pixels of the transition map within the sample box were classified as undisturbed forest); (ii) *mostly undisturbed* (fewer than five pixels have changed), and (iii) *mostly changed*. The *mostly changed* class corresponds to sample plots with (i) at least five pixels that have changed from forest to non-forest or degraded forest, and (ii) fewer than five pixels that have been classified as other land cover.

From our reference dataset, we used the Landsat interpretations at different dates (from two to four dates) (**Figure 11**) combined with the HR interpretation to obtain the following potential classes for each reference sample plot:

(i) *undisturbed forest* (no interpretation of non-forest or mosaic forest/non-forest events) both on Landsat and HR (shrubland or mosaic forest/shrubland or invalid);

(ii) forest with *major or minor disturbance only on HR* (undisturbed forest on Landsat);

(iii) forest with *major disturbance*, i.e. with at least one interpretation of major disturbances (at least five pixels) on Landsat, whatever the HR interpretation;

(iv) forest with *minor disturbance*, i.e. with at least one interpretation of minor disturbances (fewer than five pixels) on Landsat, whatever the HR interpretation.

In addition, for the sample plots with disturbances identified either from the transition map or from the reference dataset of Landsat interpretations, we identified subclasses based on the number of Landsat images interpreted as disturbed. From the transition map, we defined three subclasses based on the number of disruption observations within the box and over the full 36-year period: (i) one disruption observation, (ii) between two and three disruption observations, and (iii) more than three disruption observations. For the reference dataset of Landsat interpretations, we identified four subclasses corresponding to the number of images that were interpreted as disrupted (including major and minor disturbances), i.e. 1, 2, 3 or 4.

The numbers of disruption observations in our sample were used to analyse the omission and commission errors between the transition map and the reference dataset.

To estimate the accuracy of the transition map, we used a simplified legend that allowed a good correspondence between the classes of the transition map and of the interpretations of the reference dataset. The simplified land cover legend included two target classes: (i) *undisturbed forests* and (ii) *forest changes*. From the transition map, a sample plot was considered *undisturbed forest* when the plot box was fully undisturbed (all nine pixels of the box) and was considered *forest changes* in the other cases, i.e. when the plot box contained at least one pixel of disturbance (i.e. including minor and major disturbances). From the reference dataset, a sample plot was considered *undisturbed* when there were no disturbance interpretations either on Landsat or on HR (or an invalid interpretation on HR) and *forest changes* in the other cases, i.e. when there was at least one disturbance interpretation either on Landsat or on HR.

The contributions of the sample plots were then weighted on the basis of the stratification used in the sampling phase (see the subsection 'Sampling design' above). Finally, the user, producer and overall accuracies, the omission and commission errors, the confidence intervals of the estimated accuracies and the corrected estimates of undisturbed and disturbed forest areas with a 95% confidence interval on this estimation were computed in accordance with the good practices recommended by Olofsson *et al.* (**53**).

5 Results

5.1 Transition map

The transition map shows the spatial distribution of the moist forest at the end of the year 2019 including small linear features such as gallery forests (**Figure 13** and **Figure 14**). It depicts the sequential dynamics of changes by providing transition stages from the initial observation period to the end of the year 2019, i.e. undisturbed forest, degraded forest, forest regrowth, deforested land, conversion to plantations, conversion to water, afforestation, and changes within the mangroves, as well as the timing (dates and duration), recurrence and intensity of each disturbance.

Subsets of the transition map are presented at **Figures 14 to 19**. The detailed legend is provided in **Annex 3**. A simplified legend is provided in **Figure 14**.

Figure 13. Map of tropical moist forests remaining in January 2020 and disturbances observed during the period 1990-2019.

Legend is available in Figure 14
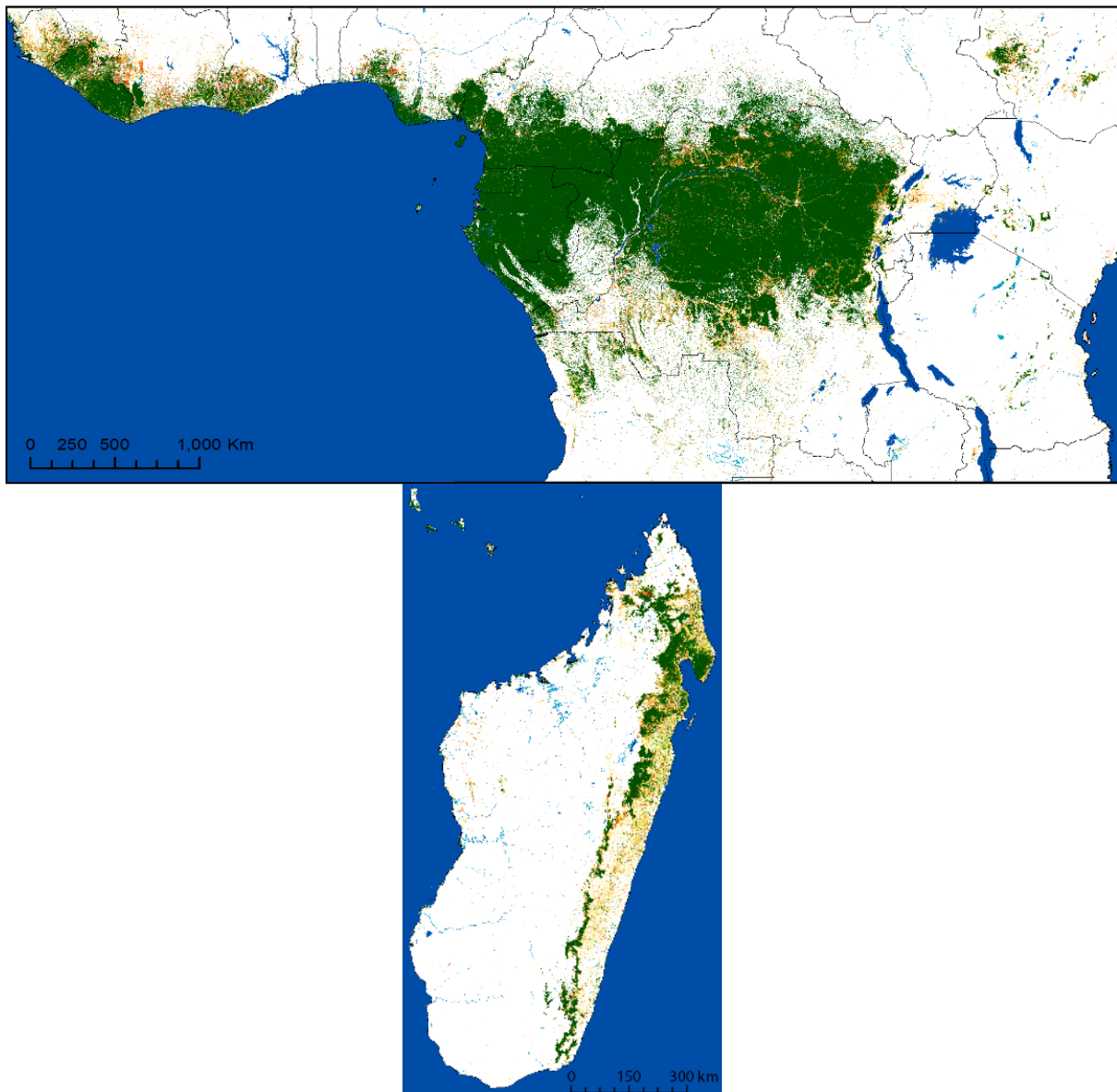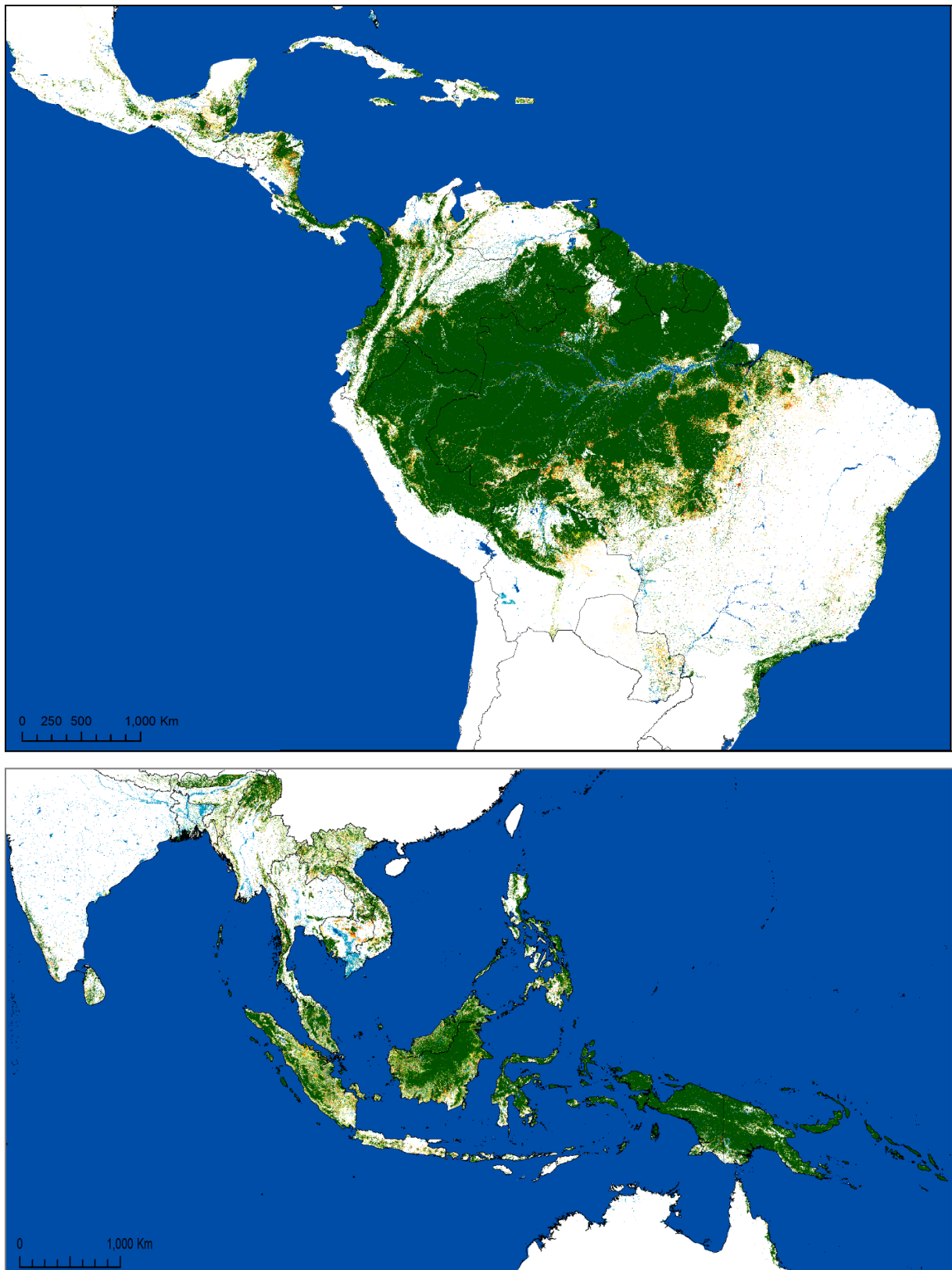
Various types of deforestation and degradation events are mapped (**Figure 14**).

Impacts of logging activities are captured with different intensity levels, from selective logging impacts, which are mapped as degraded forests with short duration of disturbance detection (**Figure 14 D and F, Figure 15**) to conversion of forest cover to another land cover (mainly pasture or crops) (**Figure 14 C and E, Figure 16**) or vegetation regrowth.

Small logging impacts such as skid trails and logging decks in concessions are also identified (**Figure 14 D and F**, **Figure 16**).

Figure 14. Examples of patterns of forest cover disturbances (deforestation and degradation) during the period 1990-2019

(A) Remaining Mangroves and the related changes in Guinea-Bissau (14.9°W, 11.1°N), (B) Fires in Mato-Grosso province of Brazil (53.8°W, 13°S), (C) Recent deforestation in Colombia (74.4°W, 0.7°N), (D) Logging in Mato-Grosso (54.5°W, 12°S), (E) Deforestation and degradation caused by the railway in Cameroon (13.4°E, 5.8°N) (F) Recent selective logging in Ouesso region of Republic of Congo (15.7°E, 1.4°N), (G) Deforestation for the creation of a dam in Malaysia (113.8°E, 2.4°S), (H) Massive deforestation in Cambodia (105.6°E, 12.7°N), and (I) Commodities in the Riau province of Indonesia (102°E, 0.4°N). The size of each box is 20 km×20 km.
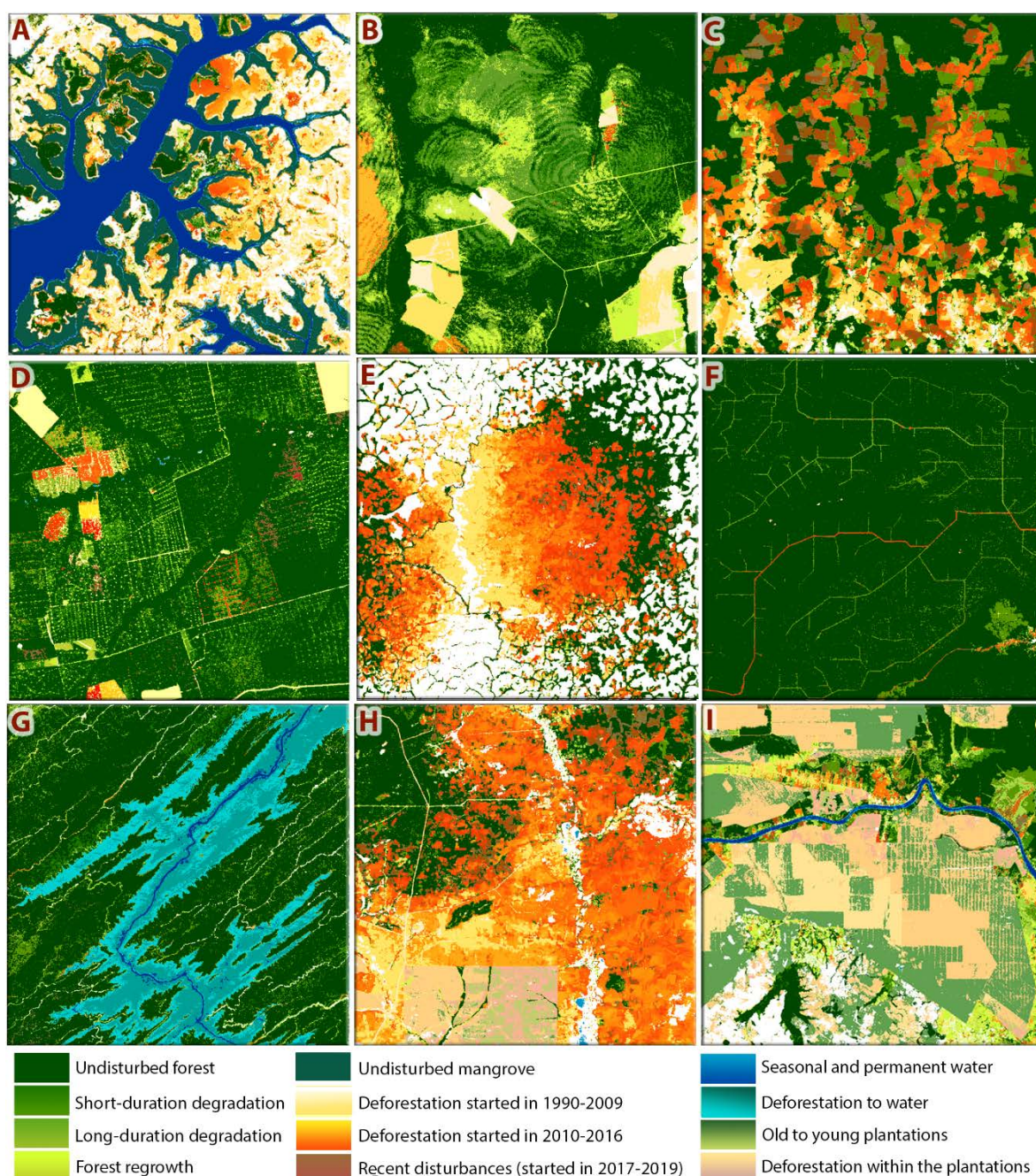
Figure 15. Subsets (10 km × 30 km) of the transition map capturing different types of logging areas

A, logging concession in Ouesso, the Republic of the Congo; B, selective logging in Para state, Brazil; C, logging network in Suriname; D, logging and deforestation in Papua New Guinea. Short-duration degradation (logging activities) appears in green and deforestation appears in red.
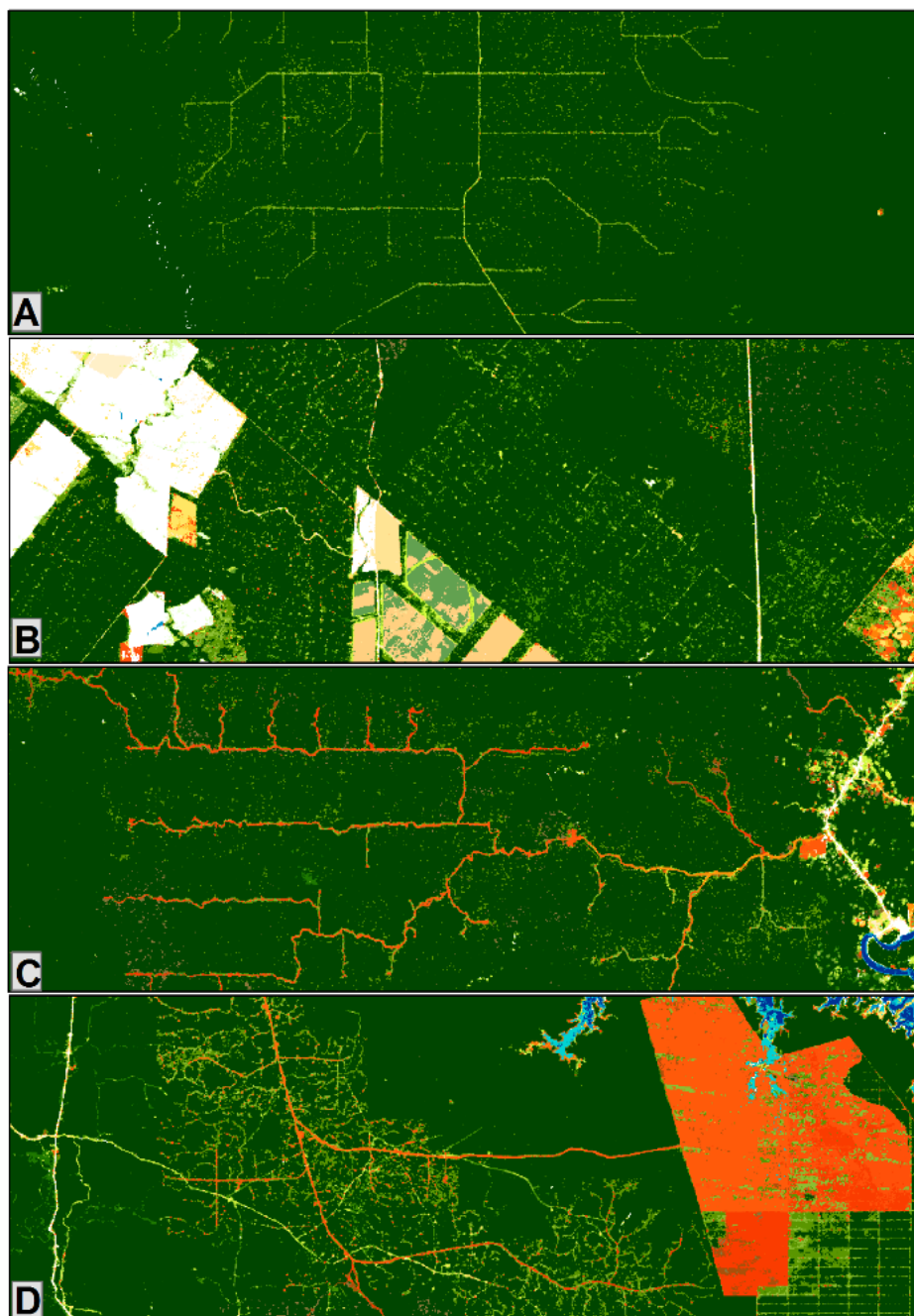
Conversion to tree or shrub plantations occurred mainly for oil palm and rubber tree in Africa and Asia (**Figure 14D, and**

Figure 17).

Small-scale agriculture also contributes significantly to the conversion and degradation of forests. This is the case in both Madagascar and the Democratic Republic of the Congo (DRC), where shifting cultivation, small tree plantations, irrigated crops, forest regrowth and dense humid forests are often present together as a 'rural complex' in landscapes around villages (**Figure 18C**) or cover major parts of the landscape (Madagascar).

In Ivory Coast, most undisturbed forests which were remaining in 2008 have disappeared, except in a few remaining protected areas (**Figure 16D**).

Figure 16. Subsets of the transition map capturing different types of deforestation processes

A, deforestation in the south of Porto Velho (Rondônia state, Brazil; B, deforestation in Roraima state, Brazil; C, deforestation and degradation due to the proximity of the railway in Cameroon; D, degradation and deforestation in a protected area in Ivory Coast. The size of each subset is 18 km × 50 km.
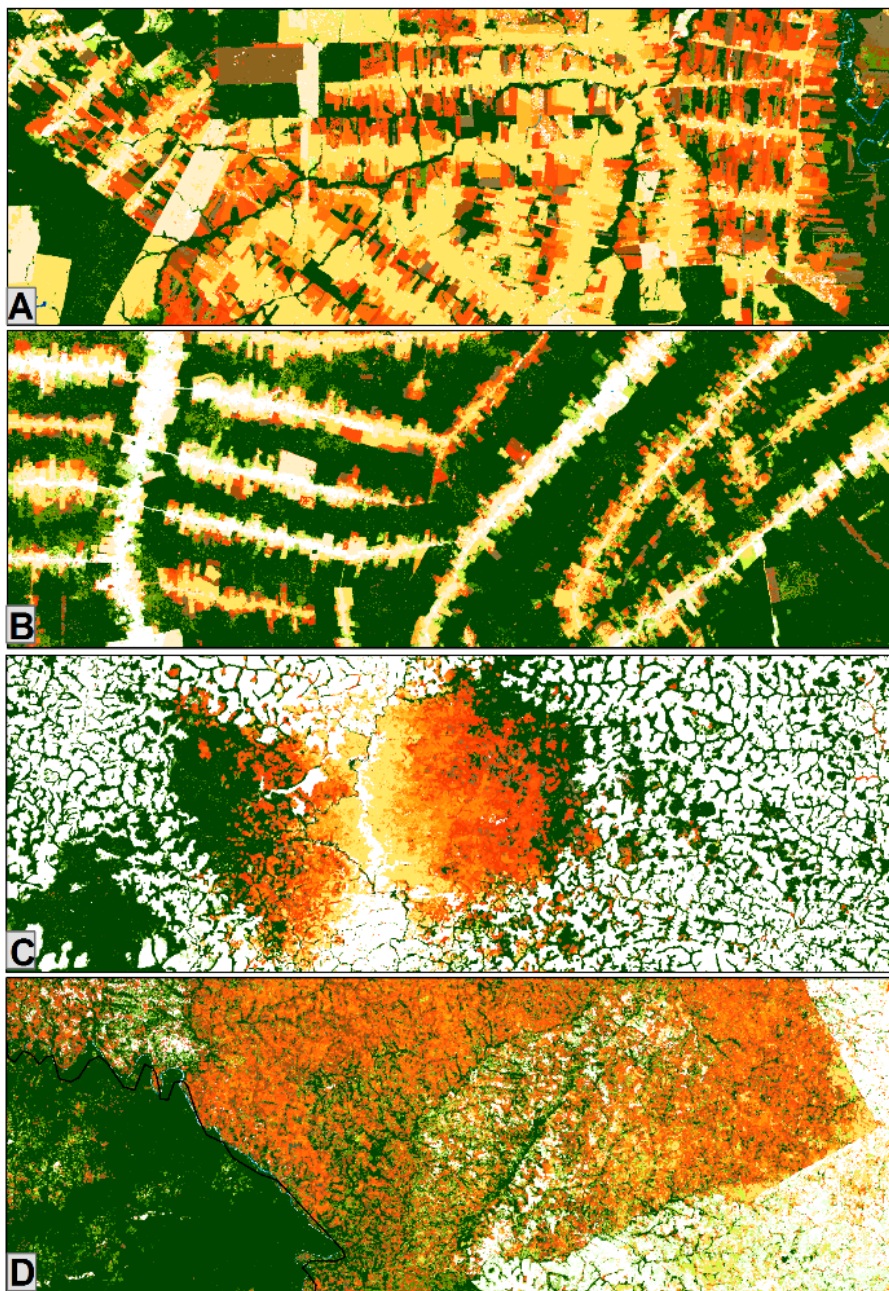
Figure 17. Subsets (18 km × 50 km) of the transition map capturing different tree plantation areas

A, cacao plantation in Venezuela; B, recent large oil palm plantation in Gabon (2015-2017); C, massive forest conversion to oil palm plantations in Cambodia; D, oil palm plantations in Indonesia.
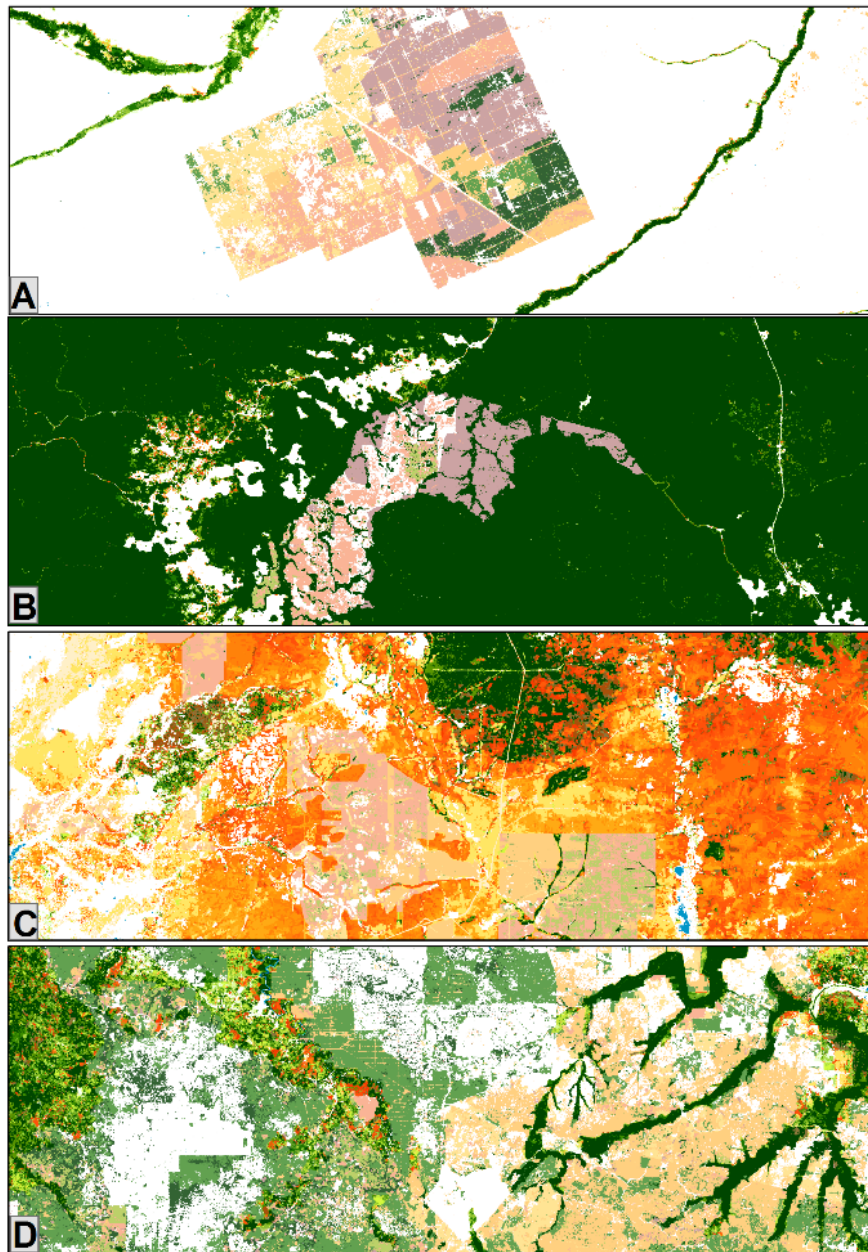
Mining exploitation of metals and precious minerals is also a cause of deforestation, such as gold mining within the dense forest, often along river courses (**Figure 18D**). The infrastructure used for petrol extraction (drilling, pipelines) in Gabon also causes damage to forests.

Strong El Niño southern oscillation (ENSO) events cause droughts and subsequently fires, which can lead to long term degradation or be followed by full death of tree cover, such as in Cambodia, where a semi-evergreen forest dried up in 2016 (**Figure 19B**). The ENSO

event that occurred in 2015-2016 caused extreme drought in the northern Brazilian Amazon and induced the burning of forest cover (**Figure 19D**).

Figure 18. Subsets (18 km × 50 km) of the transition map

A, forest conversion to water body due to a new dam in Malaysia; B, road network in Sarawak, Malaysia, at the border with Kalimantan Indonesia; C, rural complex in the Democratic Republic of the Congo; D, Gold mining in Peru (Madre De Dios, Mazuco).
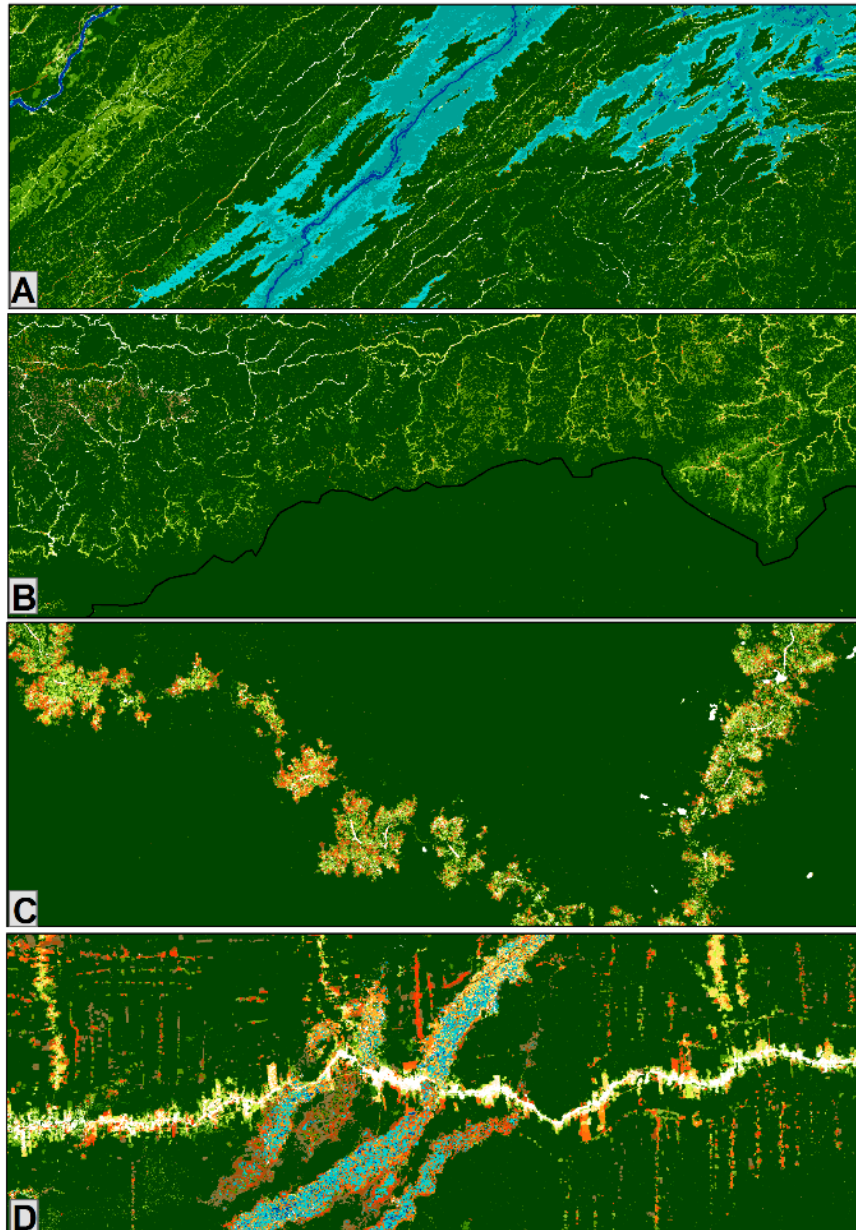
Other extreme natural events with very short durations can also cause forest damage, for example Debbie cyclone in Australia in April 2017 (**Figure 19A**), Maria hurricane in Puerto Rico at the end of 2017 or Hudah cyclone in Madagascar in April 2000 (**Figure 19C**).

Transport infrastructure such as main roads and railways is well captured on the transition map within the dense humid forest (**Figure 15C**). The impacts of new dams are identified as conversion from undisturbed forest to seasonal or permanent water (**Figure 18A**). Finally, the significant differences in forest cover patterns between bordering countries illustrate differences in resource management policies (**Figure 18B**).

Figure 19. Subsets (20 × 50km) of the transition map capturing specific degradation patterns in tropical moist forests due to climatic events

A, Cyclone Debbie in 2017 in Northern Australia; B, droughts in 2016 due to ENSO events; C, Cyclone Hudah in Madagascar in April 2000 (north of Antalaha); D, fires related to droughts in the Amazon. Degraded forests appear in light green (if occurred before 2016) or brown (in 2016 or 2017).
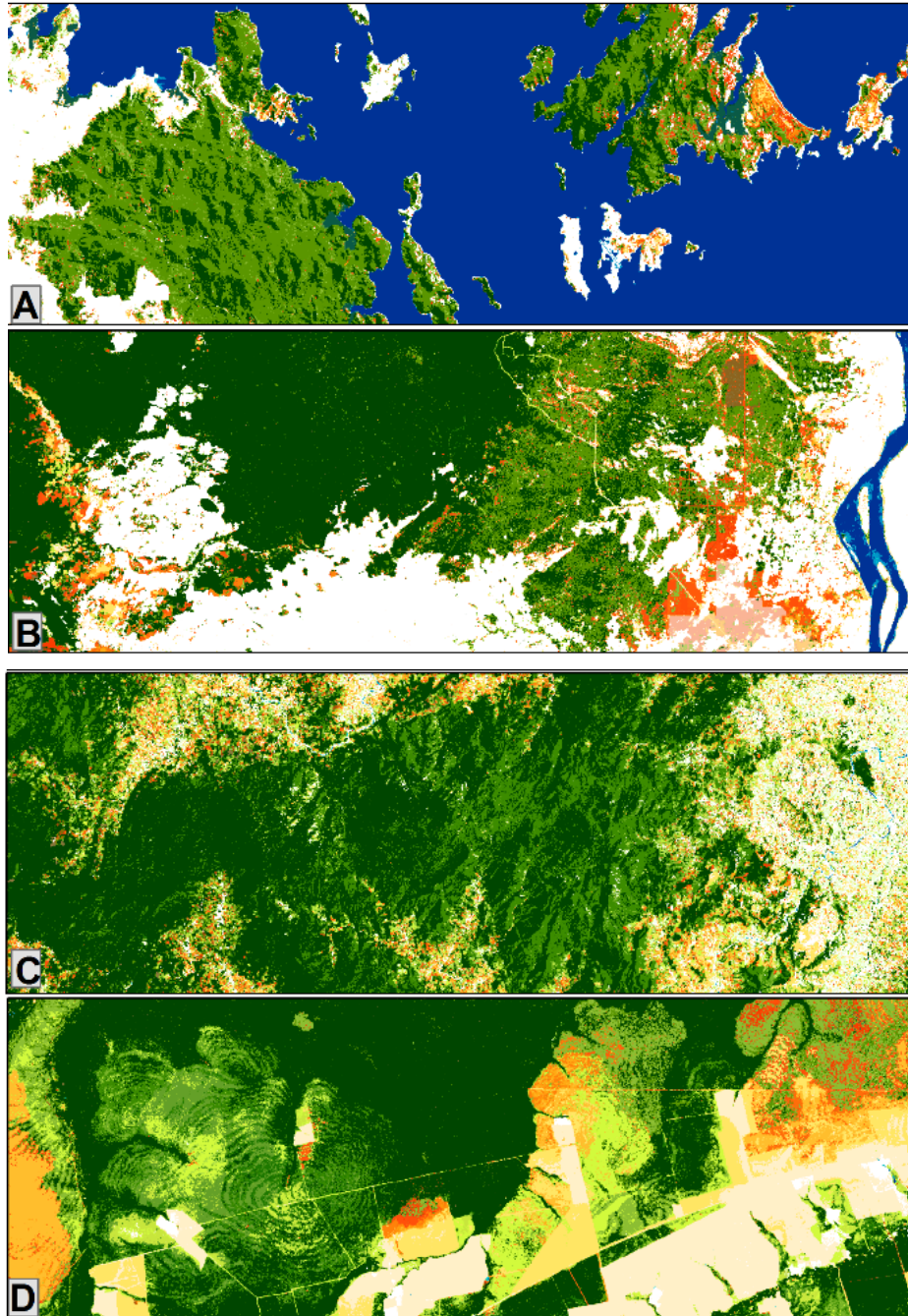
5.2 Annual change collection

The annual change dataset is a collection of 30 maps depicting - for each year between 1990 and 2019 - the spatial extents of undisturbed forests and disturbances. The annual maps depict the thirteen following classes: (i) moist forest, (ii) moist forest before the establishment of a tree plantation, (iii) bamboo dominated moist forest, (iv) new degradation (disruptions detected for the first time during the considered year), (v) ongoing degradation (disruptions started before the considered year and are still detected), (vi) degraded forest (disruptions started before the considered year and are not detected anymore), (vii) new deforestation (disruptions detected for the first time during the considered year), (viii) ongoing deforestation (disruptions started before the considered year and are still detected), (ix) new regrowth (deforestation occurred the year before and disruptions are not detected anymore), (x) regrowthing (deforestation occurred at least one year before and disruptions are not detected anymore), (xi) water (permanent or seasonal), (xii) other land cover, and (xiii) invalid observations.

Subsets of the annual change maps are presented at **Figures 20 to 23**. The detailed legend is provided in **Annex 4**.

Figure 20 illustrates the variety of classes on the annual change map, including TMF, past, ongoing degradation or deforestation, new or old regrowth. Degraded forests include degraded mangrove forests.

Figure 20. Subset of the Annual Change layer in 2018 in Indonesia

(Centre coordinates: 117.52, 2.13)
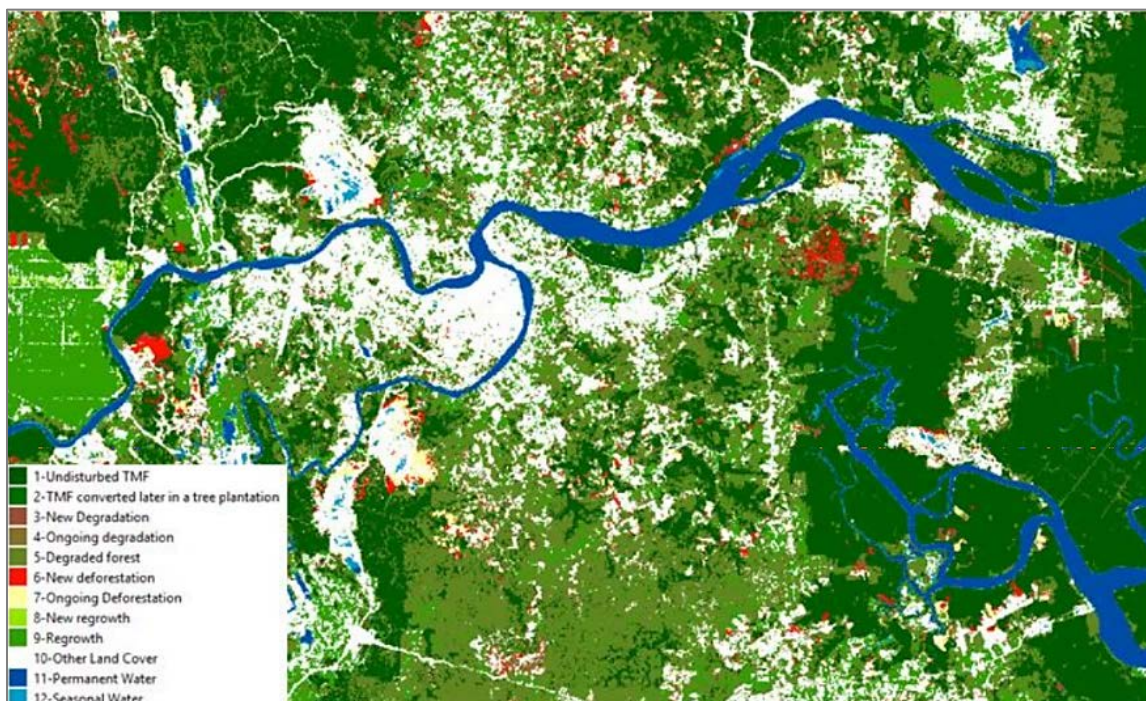
Figure 21. Subsets (25 × 34km) of the Annual Change layer at two different periods (1990 and 2015) for two regions: A, Cambodia (106 ° E, 12.5 ° N); B, Brazil - Para region (53° W, 6° S).
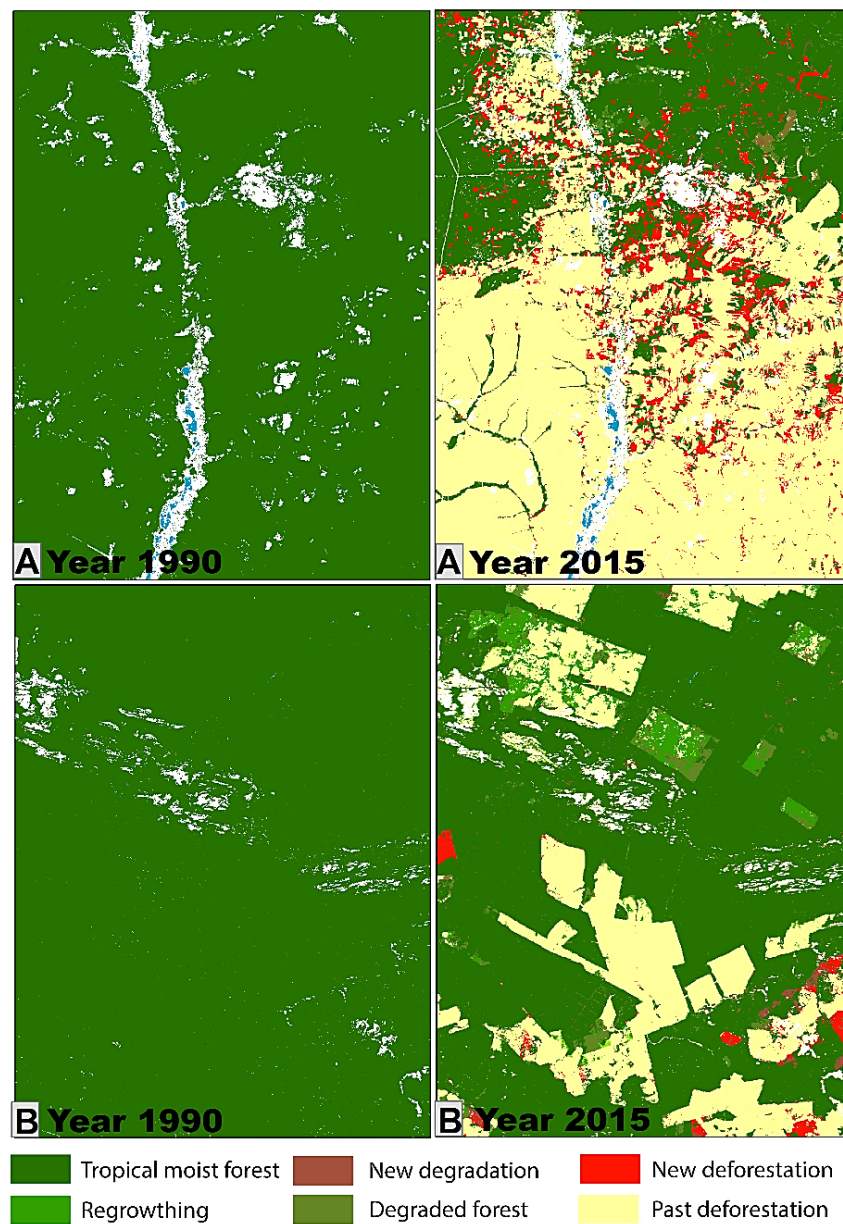
Figure 22 and

Figure 23 illustrate the changes visible from this dataset for subset regions where new deforestation and degradation occurred in 2018, in comparison with a Sentinel 2 annual mosaic of 2019 (**54**).

Figure 22. Subsets of the Annual Change layer in 2018 compared to the Sentinel 2 mosaic of 2019

Indonesia (top, centre coordinates: 117.01, 2.33) and Congo (bottom, centre coordinates: 15.47, 1.25)
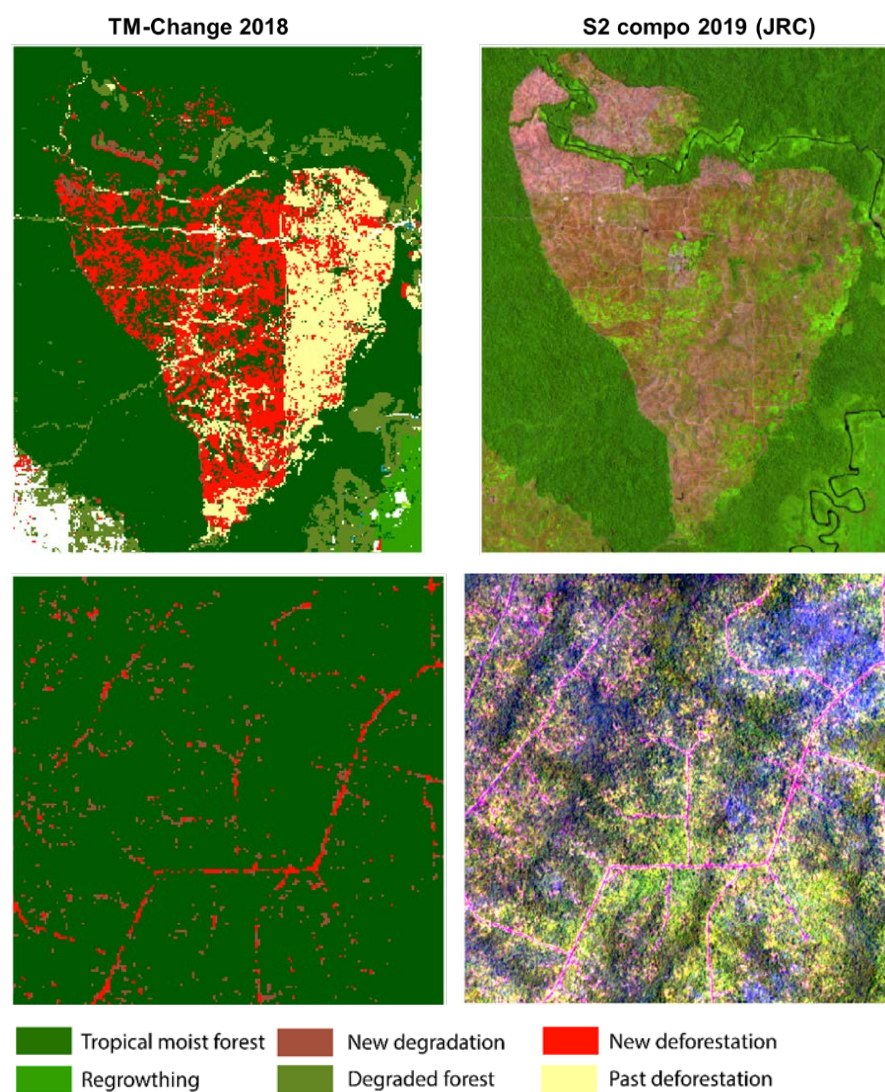
Figure 23. Subsets of the Annual Change layer in 2017 (a) and 2018 (b) in Indonesia (centre coordinates: 117.95, 2.36), compared to the Sentinel 2 mosaic of 2019 (c)

| (a) | (b) | (c) |
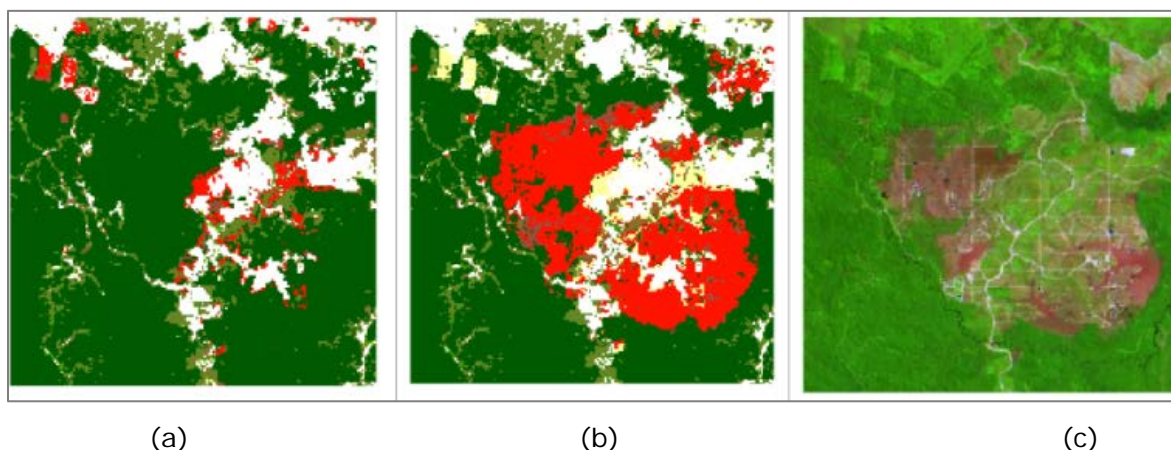
5.3 Metrics

In addition to the transition map and annual change collection, several metrics are computed and allow to characterize each disturbed pixel (degraded forest, deforested land, or forest regrowth):

j) The start and end dates of the disturbance allows identifying in particular the timing of creation of new roads or of logging activities and the age of forest regrowth or degraded forests.

k) The duration of the disturbance, i.e. the number of days between the start and end dates of the disturbance.

l) The intensity of the observed disruption events, i.e. the total number of annual disruption observations.

m) The recurrence of disruptions (in %), i.e. the ratio between the number of years with at least one disruption observation and the total number of years between the first and last disruption observations.

n) The areas that have been first degraded prior to a deforestation. Those areas are classified as *Deforested land* in the transition map.

The intensity combined with the duration, can be used as a proxy for the disturbance intensity and impact level.

5.4 Dataset flexibility and derived information

Based on the transition map, on the annual change collection and metrics produced, various information and new maps can be easily derived by selecting the type of forest to include or by selecting the year/period of interest. Some examples are given below.

A forest coverage map can be derived for a specific year (between 1990 and 2019).

Figure 24 illustrates a forest coverage map for the year 2016, which includes the undisturbed forest, the mangrove and the degraded forest.

Change areas can be mapped for a specific year or between two periods by selecting the type of changes to include, e.g. degradation and deforestation or deforestation only, deforestation that is followed or not by a regrowth, conversion to plantations, changes within the mangroves.

Figure 25 illustrates a map derived from the TMF dataset dedicated to the monitoring of the changes between 3 periods: 1990, 2005 and 2015.

Specific maps can be derived for the monitoring of the mangrove areas such as illustrated at

Figure 26 for the period 2000-2019.

By combining the transition classes and timing of the disturbance, we derived the year of degradation and the year of deforestation (**Figure 27**). Similarly, we could derive a map showing only the age of the regrowth.

Both the transition and annual change products have a detailed legend (**Annexes 3 and 4**) that can be simplified according to the user needs, e.g. by grouping all the forest regrowth classes or all the changes within the tree plantations.

Figure 24. Subsets of forest coverage derived from the Annual Change layer for several subset areas

(a) Central African Rep. (18.58, 4.20), (b) Rep. of Congo (15.67, 1.49), (c) Cambodia (108.42, 14.24), (d) Indonesia (117.73, 2.19)

1-Tropical Moist Forest
2-Degraded TM Forest
3-Mangrove
4-Degraded Mangrove
5-Plantation
6-Permanent Water
7-Seasonal Water
8-Other Land Cover

(a)　　　　　　　　　　　(b)

(c)　　　　　　　　　　　(d)
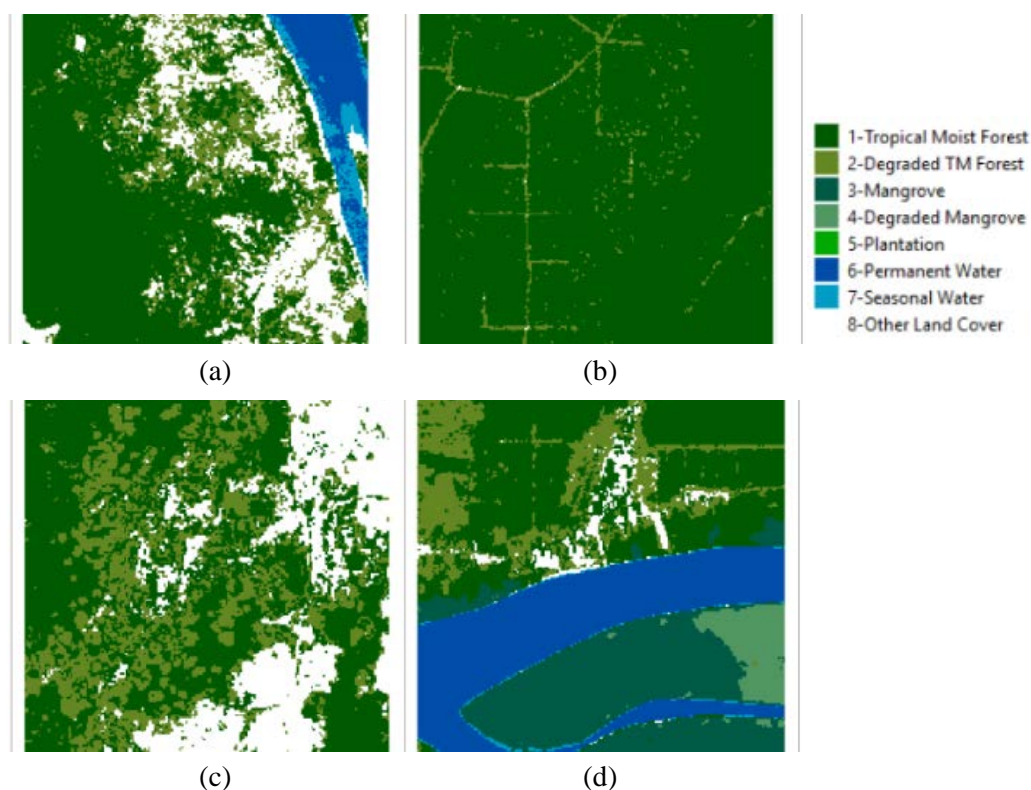
Figure 25. TMF coverage at the end of 2015 in Porto Velho, Brazil (63.28, -9.01)

Deforestation areas between 1990 and 2000 (yellow), deforestation areas between 2000 and 2015 (orange), and two classes of degraded areas (dark and light green) corresponding to 1990-2000 and 2000-2015
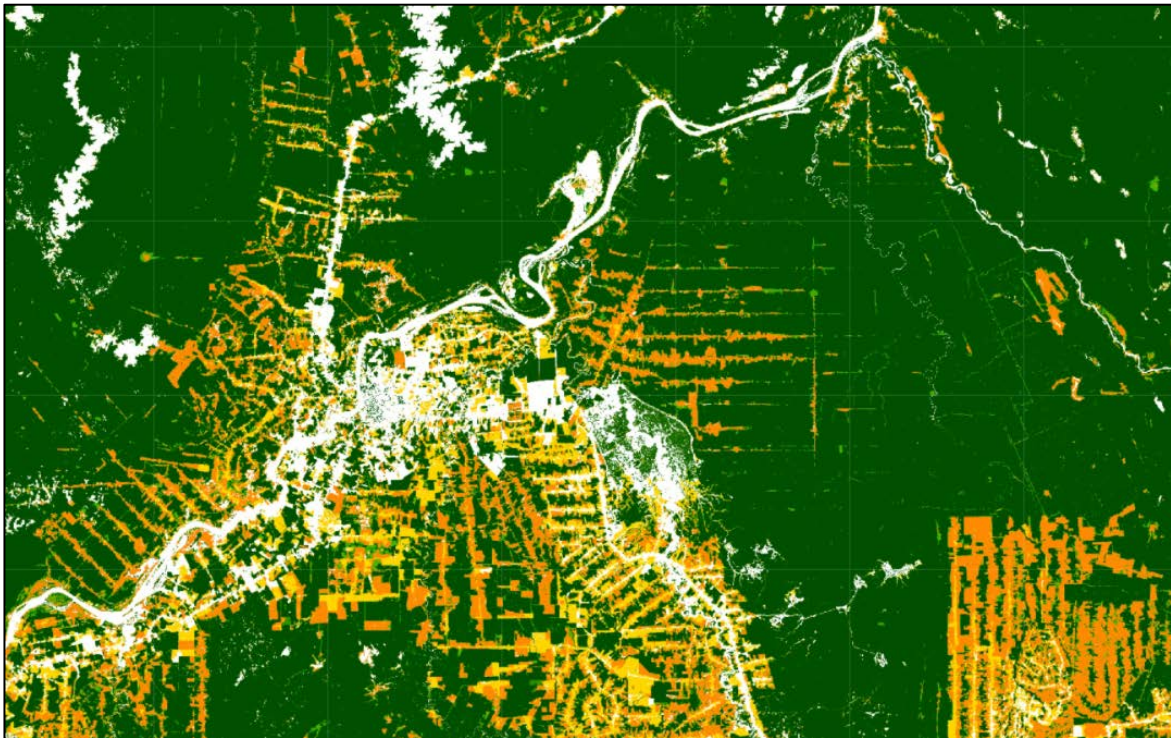
Figure 26. Maps of the undisturbed mangrove at the end of 2019

With changes that occurred within the mangrove between 2000 and 2019 for four subset areas: (a) Papua New Guinea (143.68, -8.13), (b) Colombia (-74.55, 10.87), (c) Guinea Bissau (-16.07, 12.20), and (d) Madagascar (46.12, -15.90)
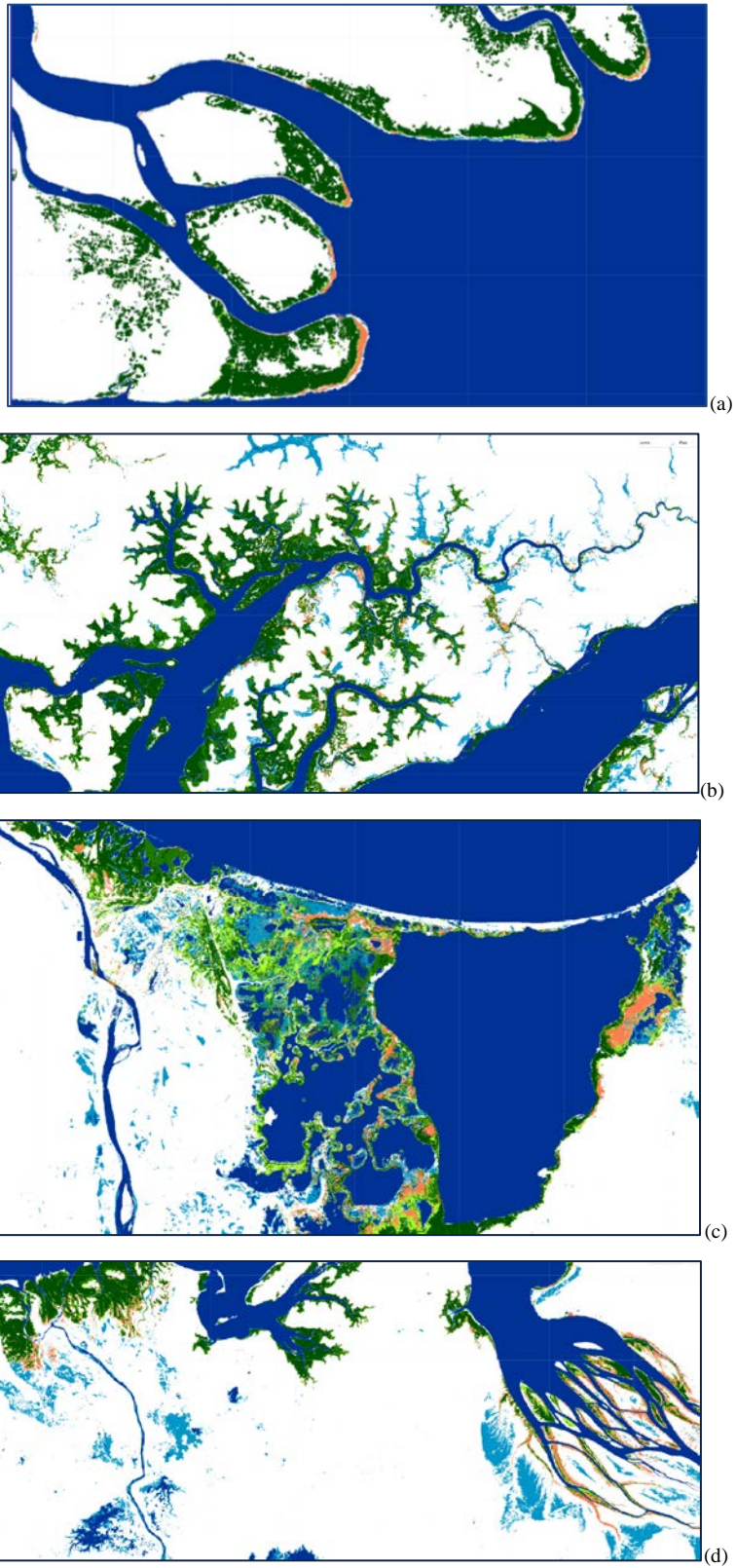
Figure 27. Year of degradation (top) and year of deforestation (bottom) in Brazil
(closed to Boa Vista, -61.73, 3.87)

1990 2019
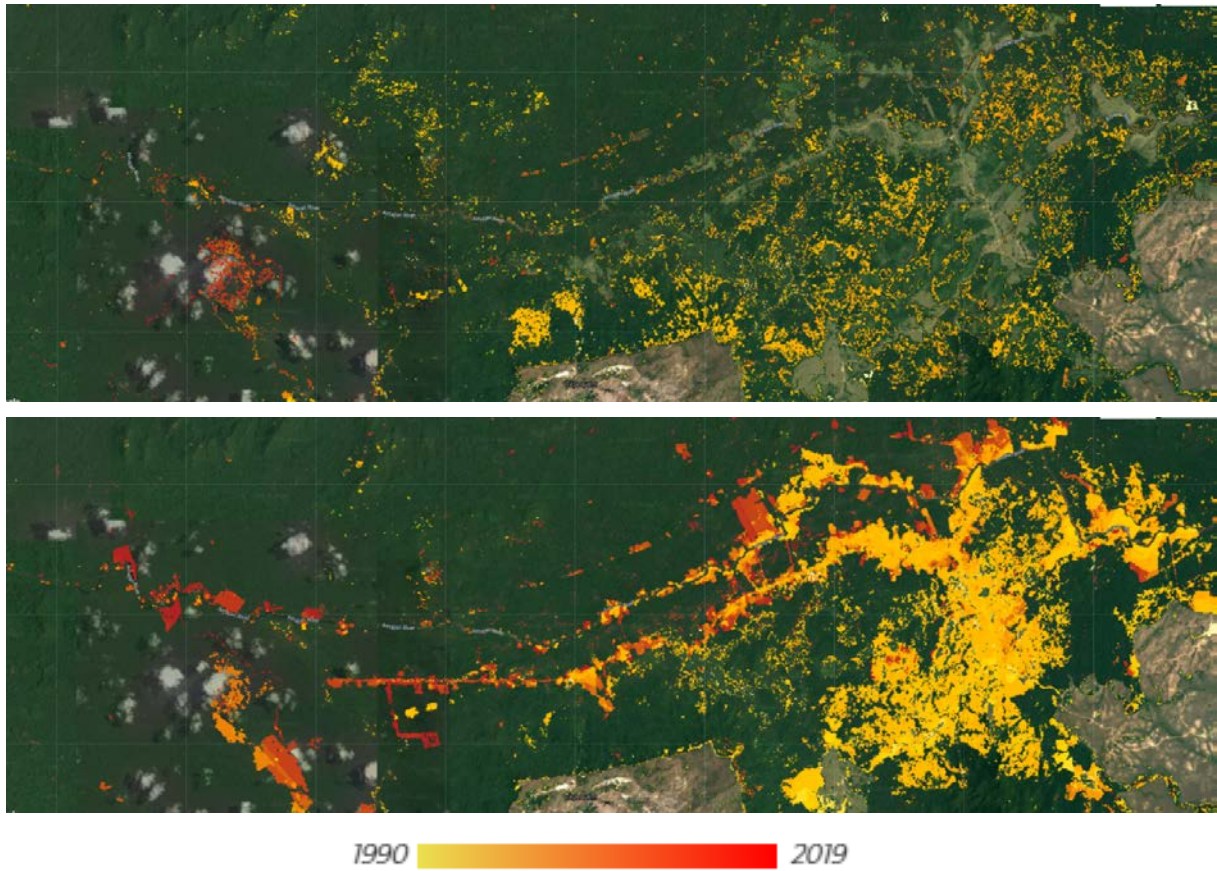
5.5 TMF Explorer

All the maps and metrics produced are freely available from the TMF explorer: https://forobs.jrc.ec.europa.eu/TMF/ (**Figure 28**). The web portal shows the transition map and the 30 annual change maps with a timeline from 1990 to 2019. Several metrics are also displayed: the years of deforestation and degradation, the duration and intensity of the disturbance, and the areas that have been first degraded prior to a deforestation.

By clicking on a pixel, we obtain the values of the various classes and metrics as well as the temporal evolution of the annual number of disruptions and valid observations.

Figure 28. Snapshot of the TMF explorer website
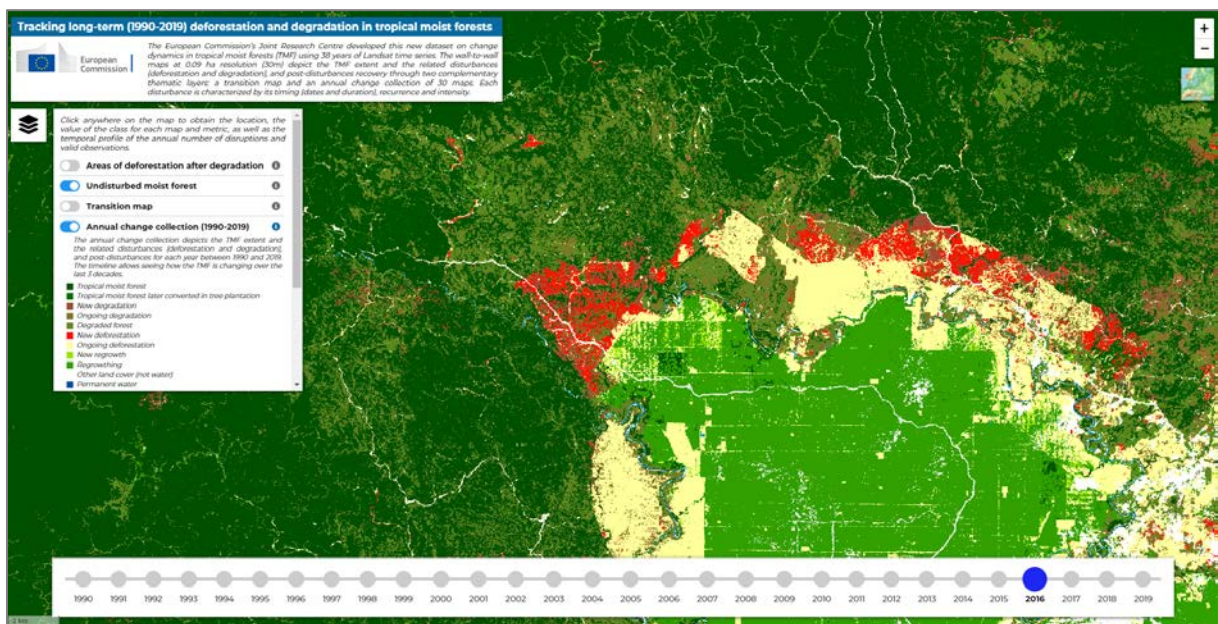
All the dataset will be accessible through FTP by tiles of 10 X 10 degrees (**Figure 29**) and in GEE when the peer-reviewed article will be published.

Figure 29. Tiling used for downloading the dataset through FTP
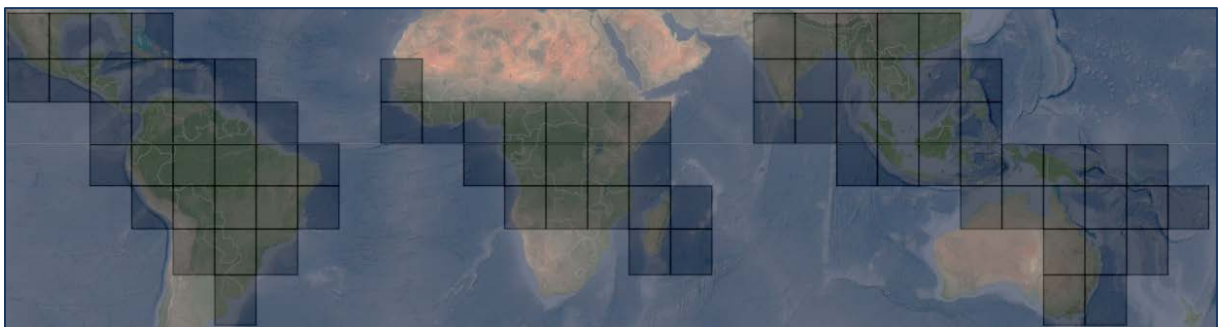
5.6 Validation

The validation was performed using a reference dataset of 5 119 sample plots with at least one valid Landsat interpretation per plot (1 705 for Africa, 1 693 for Asia and 1 700 for Latin America) and a total of 12 343 Landsat interpretations (3 823 for Africa, 4 215 for Asia and 4 305 for Latin America) distributed temporally (across the period 1982-2016) and across Landsat sensors (L5, L7, and L8). The 12 343 Landsat interpretations were compiled from the 5 119 sample plots using Landsat images at selected dates with no cloud presence, no sensor artefacts and no doubt about the visual interpretation (from one to four Landsat images per plot). Within the full sample of the 5 119 reference plots, 3 982 sample plots had one valid recent HR interpretation, 3% of the plots had one valid Landsat interpretation, 30% had two valid Landsat interpretations, 57% had three valid interpretations and 10% had four valid Landsat interpretations.

Two confusion matrices were produced from the reference sample dataset: one from all valid Landsat interpretations (12 343 in total), to assess the performance of the single-date classification algorithm, and another from the 5 119 sample plots, to assess the accuracy of the transition map.

5.6.1   Performance of the single-date algorithm

The confusion matrix for the single-date classification (**Tables 1 and 2**) reports an overall accuracy of 91.4%, with omission and commission errors for non-forest cover detection of 9.4% and 7.9%, respectively. At continental level, overall accuracy is higher for Africa (94.6%) than for Latin America (91.0%) or Asia (89.0%). Among the 577 plots that correspond to the omission errors, 86% were classified as forest changes or other land cover on the transition map. Moreover, 71% of these plots were confirmed as changes by the HR interpretations. This shows that most of the omissions of the single-date classification algorithm were 'temporary' omissions, as most of these disturbances were then confirmed from the full temporal Landsat time series. These probably correspond to omissions at the beginning of disturbance events. It is also important to mention that 87% of these omissions were plots with minor non-forest extent (fewer than five pixels interpreted as non-forest within the sample plot).

Table 1. Accuracy matrix for all the single-date interpretations (12,345 sample plots) by continent:

a)   detailed matrix with all Landsat and HR classes;

Reference	Landsat Mostly non-forest																							
	HR Mostly non-forest				Minor non-forest				Shrub				Forest				Invalid				Total points User			
User map	AFR	Asia	SAM	Tot	AFR	Asia	SAM	Tot	AFR	Asia	SAM	Tot	AFR	Asia	SAM	Tot	AFR	Asia	SAM	Tot	AFR	Asia	SAM	Tot
Mostly non-forest	234	171	236	641	77	60	84	221	104	84	77	265	37	40	93	170	58	167	65	290	510	522	555	1587
Minor non-forest	53	64	58	175	36	16	16	68	23	21	11	55	9	9	17	35	27	64	21	112	148	174	123	445
Forest	0	29	14	43	2	4	1	7	3	6	5	14	3	1	1	5	2	7	0	9	10	47	21	78
Total points Producer	287	264	308	859	115	80	101	296	130	111	93	334	49	50	111	210	87	238	86	411	668	743	699	2110

Reference	Landsat Minor non-forest																							
	HR Mostly non-forest				Minor non-forest				Shrub				Forest				Invalid				Total points User			
User map	AFR	Asia	SAM	Tot	AFR	Asia	SAM	Tot	AFR	Asia	SAM	Tot	AFR	Asia	SAM	Tot	AFR	Asia	SAM	Tot	AFR	Asia	SAM	Tot
Mostly non-forest	139	94	70	303	171	95	200	466	149	84	129	362	40	34	69	143	58	130	42	230	557	437	510	1504
Minor non-forest	141	107	58	306	209	150	218	577	243	157	134	534	71	41	89	201	137	229	46	412	801	684	545	2030
Forest	23	39	18	80	56	61	76	193	34	28	8	70	9	8	5	22	9	120	5	134	131	256	112	499
Total points Producer	303	240	146	689	436	306	494	1236	426	269	271	966	120	83	163	366	204	479	93	776	1489	1377	1167	4033

Reference	Landsat Forest																							
	HR Mostly non-forest				Minor non-forest				Shrub				Forest				Invalid				Total points User			
User map	AFR	Asia	SAM	Tot	AFR	Asia	SAM	Tot	AFR	Asia	SAM	Tot	AFR	Asia	SAM	Tot	AFR	Asia	SAM	Tot	AFR	Asia	SAM	Tot
Mostly non-forest	4	0	1	5	7	5	14	26	9	9	50	68	1	5	17	23	0	19	2	21	21	38	84	143
Minor non-forest	5	3	6	14	20	20	33	73	11	28	64	103	6	26	47	79	2	46	20	68	44	123	170	337
Forest	62	86	63	211	219	224	244	687	244	499	169	912	824	434	1399	2657	252	691	310	1253	1601	1934	2185	5720
Total points Producer	71	89	70	230	246	249	291	786	264	536	283	1083	831	465	1463	2759	254	756	332	1342	1666	2095	2439	6200

b) simplified matrix with non-forest and forest classes.

Reference	Non-forest				Forest				
User map	AFR	ASIA	Latin-Am	Tot	AFR	ASIA	Latin-Am	Tot	Tot User
Non-forest	2016	1817	1733	5566	65	161	254	480	6046
Forest	141	303	133	577	1601	1934	2185	5720	6297
Total Producer	2157	2120	1866	6143	1666	2095	2439	6200	12343

Table 2. Accuracy results by continent and Landsat sensor.

Class	Non-Forest				Forest			
Continent	Africa	SE Asia	South Amer.	Total	Africa	SE Asia	South Amer.	Total
% Omission	6.5	14.3	7.1	9.4	3.9	7.7	10.4	7.7
% Commission	3.1	8.1	12.8	7.9	8.1	13.5	5.7	9.2
% Overall Accuracy	94.6	89.0	91.0	91.4				

Class	Non-Forest				Forest			
Sensor	LC8	LE7	LT5	Total	LC8	LE7	LT5	Total
% Omission	9.7	9.4	9.8	9.6	13.2	7.2	5.2	7.7
% Commission	10.9	7.8	6.1	8.1	11.8	8.7	8.3	9.2
% Overall Accuracy	88.7	91.8	92.7	91.4				

The accuracy matrices by continent (**Table 2**) show a higher rate of omission errors for Asia (14.3%) than for Africa or Latin America (6.5% and 7.1%, respectively) but no significant differences were observed among sensors (9.8% for LT5, 9.7% for LC8, 9.4% for LE7).

These omission errors (in the single-date classification) mainly appear as other land cover class on the transition map (49% of these omissions), but also as mostly undisturbed (a spatial majority of undisturbed forest within the box) (25%), deforestation without regrowth (17%) and mostly degraded or regrowth (10% altogether). The 577 sample plots presenting omission errors are sites of intensive disturbances, as 71% of these errors concern sample plots where the total number of disturbances detected over the 37 years was greater than three.

Among the commission errors in the single-date classification corresponding to forest cover in Landsat interpretations and non-forest cover in the single-date classification (480 plots), only 22% were interpreted as forest using the HR images, whereas 24% were interpreted as mostly or minor non-forest, 35% as shrubland and 18% as invalid. Therefore, a large part of these 'false detections' of single-date disturbance events were observed as disturbances in the most recent HR images. This raises the issue of the potential limitations of the visual interpretation of Landsat images.

Among the sample plots that correspond to these commission errors, 69% were classified in the transition map as spatial minor changes (fewer than five pixels within the 3 × 3 pixel box) and 31% as spatial major changes (more than five pixels within the 3 × 3 pixel box). In addition, of the total commission error plots, 67% concern deforestation and other land cover classes; degradation and regrowth represent 18%; and classes of mostly undisturbed forest (between five and eight pixels of undisturbed forest within the 3 × 3 pixel box) represent 15%.

More commission errors are observed for Latin America (13.2%) than for Asia (8.3%) or Africa (3.2%). These differences can be partly explained by the numbers of Landsat scenes that were processed: 540 634 scenes for Latin America, 482 965 scenes for Asia and 231 087 scenes for Africa. A larger number of scenes may result in a greater number of errors in the final product as a result of the presence of noise or artefacts within a minor part of the Landsat dataset, which cannot fully be eliminated.

Finally, more commission errors were observed for L8 (11.3%) than for L7 (8.2%) or L5 (7.3%) (**Table 2**).

5.6.2 Accuracy of the transition map and area estimates

The accuracy matrix for the transition map shows an overall accuracy (stratum-weighted estimate) of 92.8% for the classes of the moist forest domain (**Tables 3 and 4**). The omission and commission errors for the forest changes areas are 19% and 8.4%, respectively.

The commission errors concern mainly (66.3%) minor disturbances on our transition map (fewer than four disturbances detected over the observation period and fewer than five pixels within the sample plot). Of these commission errors, 24.2% concern major disturbances (more than five pixels within the plot with at least three detections over the full period).

The omission errors concern mainly (74.1%) minor disturbances that were identified only once from the valid Landsat images or disturbances that were identified only using the HR images (15.9%).

The accuracy matrix for the transition map allows us to produce reference-corrected area estimates (**Table 3**). The correction shows that a direct area measurement from the transition map underestimates the forest area changes by 38.4 million ha (325.2 million ha derived from the map versus 363.6 million ha for the corrected estimate), representing a relative bias of 11.8%, with a confidence interval (95%) of this error estimation at 15 million ha.

Table 3. Area-weighted confusion matrix for the transition map and a validation reference dataset of 4 139 sample plots (%).

Transition map	Max N disruptions	Forest on Landsat & HR	Forest on Landsat & non-forest on HR	At least 1 minor disruption on Landsat				At least 1 major disruption on Landsat				total
Reference		0	0	1	2	3	4	1	2	3	4	
Undisturbed (0pix)	0	48.0	0.6	2.6	0.2	0.0	0.0	0.2	0.0	0.0	0.0	52
Mostly Undisturbed (1-4pix disturbed)	1	1.5	0.1	0.6	0.1	0.0	0.0	0.1	0.0	0.0	0.0	2
	2-3	1.2	0.2	0.4	0.1	0.0	0.0	0.0	0.0	0.0	0.0	2
	>3	0.2	0.1	0.7	0.4	0.2	0.1	0.4	1.0	6.6	2.3	12
Mostly changed (5-9pix disturbed)	1	0.4	0.1	0.2	0.0	0.0	0.0	0.0	0.0	0.0	0.0	1
	2-3	0.6	0.1	0.6	0.2	0.0	0.0	0.2	0.3	0.0	0.0	2
	>3	0.2	0.1	2.2	1.4	1.1	0.0	3.3	9.4	11.2	0.4	29
Total		52	1	7	2	1	0	4	11	18	3	100

Table 4. Area-weighted matrix showing the transition map versus the reference dataset and error estimation (million ha).

Areas (million ha)	Reference		
Transition map	Undisturbed forest	Forest Change	Total area
Undisturbed Forest	898.6	65.8	964.4
Forest Change	27.4	297.8	325.3
Total area	926.0	363.6	1289.6
Errors (million ha)			
Commission error	65.8	27.4	
Omission error	27.4	65.8	
Difference	-38.4	38.4	
CI (95%)	14.8	14.8	

6 Discussion: Specificities and added value of the TMF product

The main specificities and added values of the TMF dataset are described below:

- The TMF dataset covers a long-term monitoring period (1990-2019) on an annual basis with an effective observation period that varies at the pixel level (see **Sections 3 and 7**).

- For the first time at the pantropical scale the occurrence and extent of the forest cover degradation is mapped on an annual basis in addition to the deforestation. This has been achieved thanks to the analysis of each individual valid observation of the Landsat archive images (vs annual syntheses or intra-annual statistics used in previous studies, see Data and Mapping method Sections) allowing to capture short-duration disturbances such as selective logging, fires, and severe weather events (hurricanes, dryness).

- All the changes are characterized based on (i) sequential dynamics (by providing transition stages from the initial observation period to the end of the year 2019), (ii) timing (dates, duration), (iii) intensity (total number of disruptions detected), and (iv) recurrence.

- The TMF coverage has been mapped at the pan-tropical scale in a consistent way for each year over the last three decades. As specified in Section 2, we did not intent to map specifically intact or primary forest as the Landsat observation period is too short to discriminate never-cut primary forest from second growth naturally recovered forest older than the observation period. However, by documenting all the disturbances observed over the last three decades, the remaining undisturbed TMF in 2019 is getting closer to the primary forest extent.

- The identification of several forest cover change classes compared to the global monitoring of forest clearance:
  - 3 main change trajectories: degradation, deforestation and regrowth,
  - Deforestation is documented in an unprecedented comprehensive manner,
    - by mapping deforestation occurring after degradation and deforestation followed by a regrowth,
    - by identifying specific forest conversion to commodities/tree plantations and conversion to permanent/seasonal water (e.g. creation of a dam),
    - by including changes within the mangroves.
  - Sub-classes are identified based on the duration and intensity of the disturbance. Three decadal periods have been used in the transition map to identify age sub-classes of degradation and forest regrowth: (i) before 2000, (ii) within 2000-2009 and (iii) within 2010-2019.

Figure 30 and 31 illustrate the detail of the TMF product compared to the GFC loss data:

c) TMF data capture deforestation or degradation events that occurred before 2000 compared to the GFC loss product that covers the period 2001-2019, e.g. old deforestation areas converted in agriculture mostly in 1997 (light pink on the TMF map in panel B of **Figure 30**).

d) TMF data discriminate degraded areas from deforested areas whereas GFC product shows a loss for all disturbance types (with the year of the loss), missing one part of the degradation and misclassifying degraded forest (canopy gaps) as deforested land (in panels A and B of **Figure 30**). In logging concessions (in panels A and C of **Figure 30**), TMF discriminates the main roads (deforested in orange) still used to access new logging concession from old logging roads (now regrowthing in light green), from canopy gaps (degraded forest) between the logging roads (dark green).

e) TMF data discriminate burned areas (classified as forest regrowth, in light green or degraded forest in dark green) from deforested areas (main roads or conversion to agriculture) and tree plantations (in panels A and C of **Figure 30**).

f) TMF data well capture the changes within the mangrove whereas most of these changes are missed on the GFC product (**Figure 33**).

g) TMF data discriminate three types of forest clearance: (i) forest areas that have been converted in seasonal or permanent water (e.g. creation of a dam), (ii) forest areas that have been converted to tree plantations, (iii) deforested areas (converted in agriculture or infrastructure), whereas GFC show only one type of disturbance (**Figure 30 C**).

Figure 30. Comparison between the TMF transition map (1990-2019) and GFC loss year (2001-2019)

Panel A in the Ouesso region of the Republic of Congo
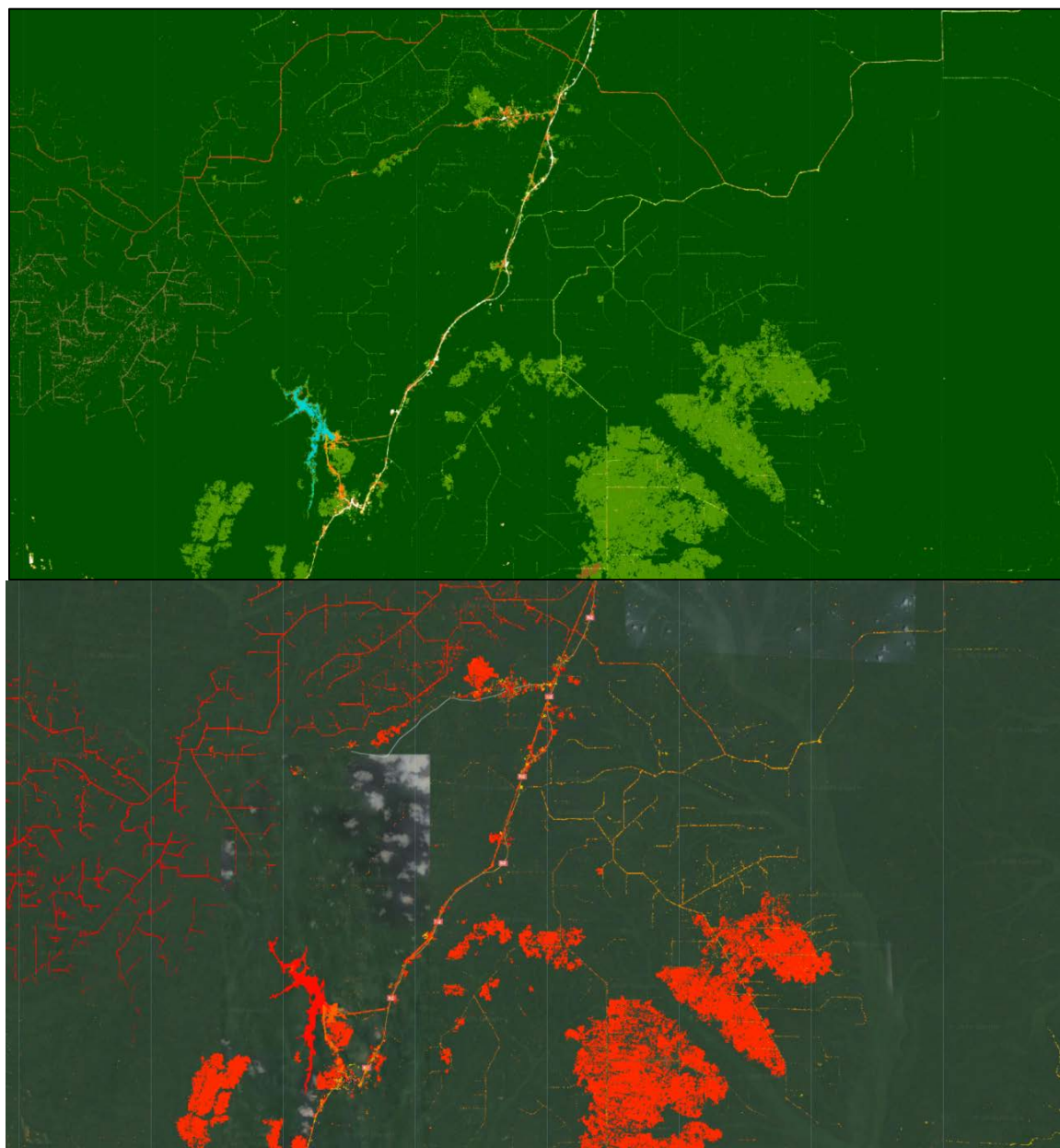
Figure 31. Comparison between the TMF transition map (1990-2019) and GFC loss year (2001-2019)

Panel B in Mato Grosso (Sinop), Brazil (-54.0427, -11.1829)

Figure 32. Comparison between the TMF transition map (1990-2019) and GFC loss year (2001-2019)

Panel C in Borneo (113.9881, 2.6494)
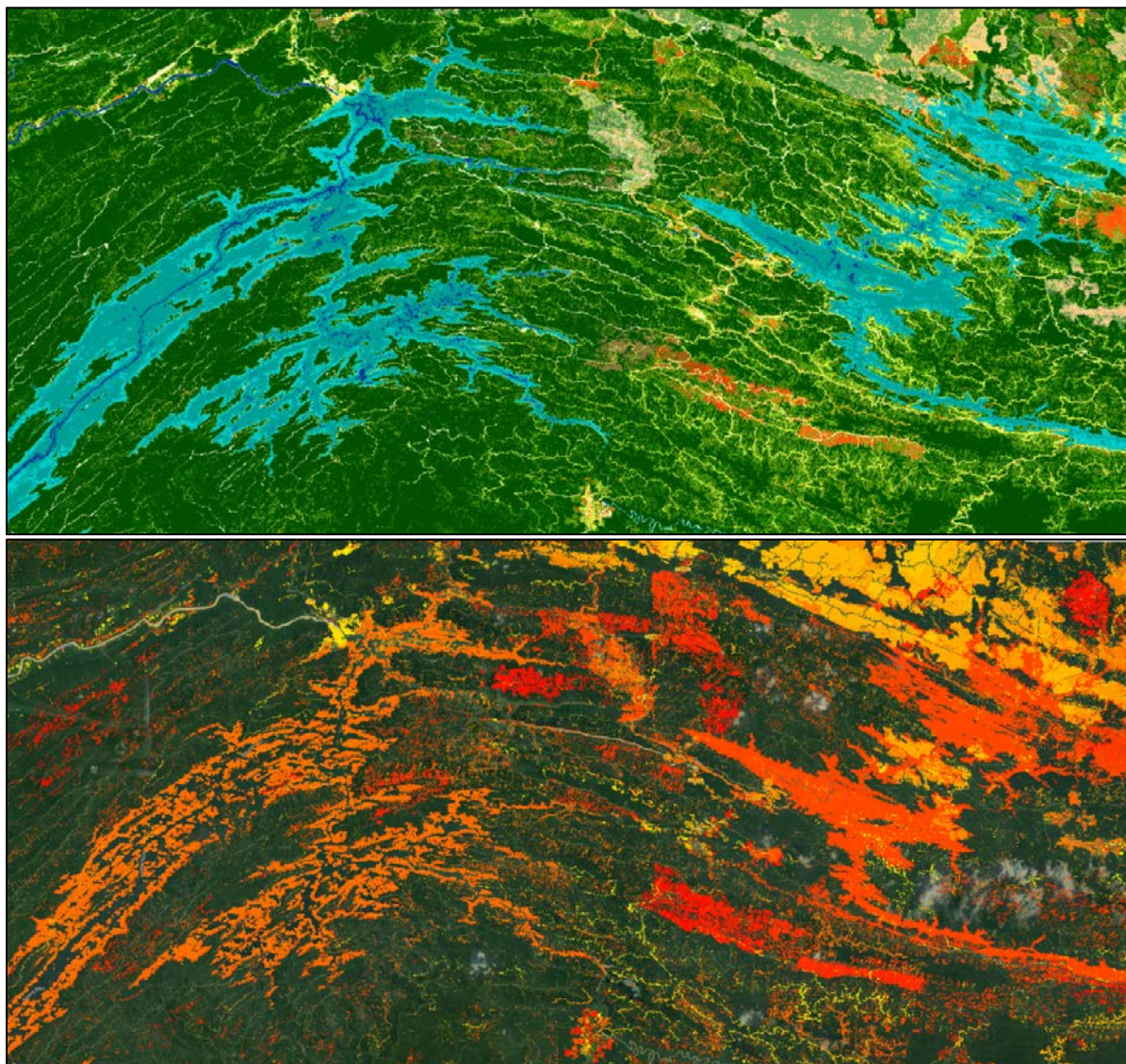
Figure 33. Comparison between the TMF transition map (right), the GFC losses (2001-2018) in black, and the Google Earth HR imagery of 2005 and 2018, in Guinea-Bissau (8.951,-13.244)

Google Earth – January 2005   Google Earth – December 2018   TMF change (colors) & GFC loss (black)
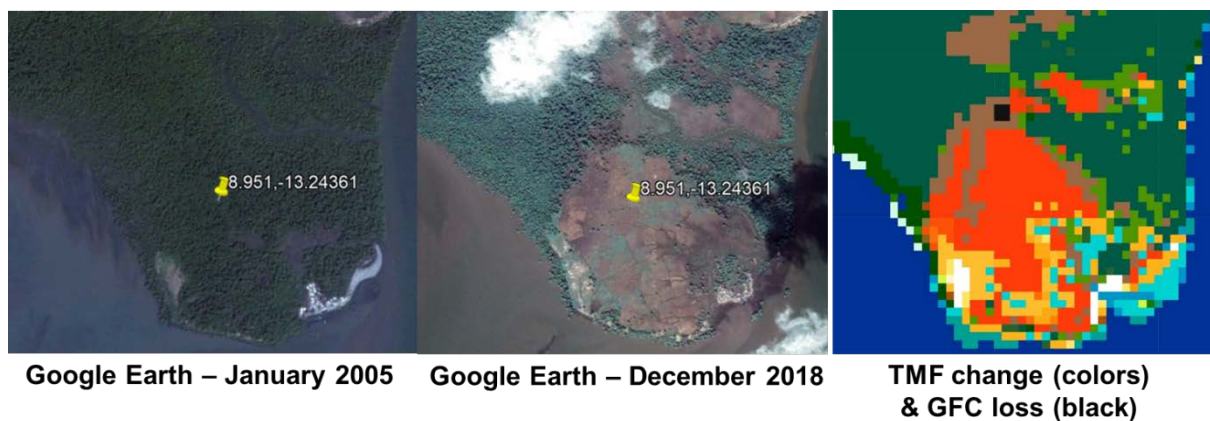
7 Known limitations and future improvements

Disturbances that affect less than the full pixel area (0.09 ha size), e.g. the removal of a single tree, are generally not included in our results because the impact of the spectral values of the pixel are not strong enough to be detected. However, in specific cases, where the impact on the forest canopy cover modifies significantly the spectral values within a single pixel, e.g. the opening of a narrow logging road (< 10 m wide) or the removal of several big trees, our approach can detect such disturbances.

We have addressed the geographic and temporal discontinuities of the Landsat archive (see Data and Mapping method) by determining at the pixel level (i) an initial period (baseline) of minimum four years (increasing when the annual number of valid observations is low) for mapping the initial TMF extent and (ii) a monitoring period for detecting the changes. This minimizes the risk of inclusion of non-forest cover types (such as agriculture) and deciduous forests in the baseline when there are few valid observations over a short period. This risk has been under-estimated by previous studies that did not use a long period of analysis and did not accounted for the number of valid observations.

The accuracy of the disturbance detections has been assessed in the validation exercise (see Validation section). The assignment of the disturbance types at any location improves as the number of valid observations increases. The meta-information documents (i) the annual number of valid observations (ii) the first year of valid observation (**Figure 3**) and (iii) the start year of the monitoring period (**Figure 8**) at each pixel location. This meta-information (in particular the number of valid observations) can be considered as a proxy measure of confidence. Hence our estimates of changes in the regions where the total number of valid observations is particularly low and/or the start year of the monitoring period is late (**Figure 2, 3, and 8**), e.g. Gabon, Salomon Islands, La Reunion, should be considered with lower confidence. However, considering the geographic completeness of Landsat-8 coverage after year 2013 there is high confidence for the contemporary reported estimates.

For the first time at pan tropical scale, a fine spatial resolution and annual frequency, detailed information on the historical forest area changes within the plantation concessions of oil palm and rubber are provided through to the combination of ancillary information and dedicated visual interpretation (**Annex 1**). Although some confusion between forests and old plantations may remain (in particular for plantations that are not included in the ancillary database of concessions or that cannot be easily identified visually on satellite imagery from a regular geometrical shape), such errors are expected to be limited due to the consideration of (i) a minimum duration for the initial period and (ii) a long observation period. Classes of tree plantations do not include all commodities such as coffee, tea and coconut, that are detected as deforested land (if initially TMF and converted in commodity during the monitoring period) or other land cover (if the concession was already established during the initial period).

Some isolated commission errors may remain in the bamboo-dominated TMF, wetlands and semi-deciduous forests as reference data were available on restricted areas (**Annex 2**). These will be continuously improved as the reference information layers improve and based on the feedback of users and national authorities.

The L7 SLC-off issue may introduce some spatial inconsistencies owing to a higher number of valid observations outside the SLC-off stripes which allows more disruptions to be captured and leads – potentially - to a different transition class.

Efforts have been done to classify disturbances based on their characteristics (timing, recurrence and sequence) in order to fit to the land cover use. However, all the metrics used in this study are made freely available to the end-user to possibly apply different decision rules that would better fit to the specific user needs and constraints, e.g. threshold applied to discriminate deforestation from degradation may be different according to the selected definition of the degradation.

This approach can be automatically applied to future Landsat data (from 2020) and is intended to be adapted to Sentinel 2 data (available since 2015) towards a monitoring of tropical moist forests with higher temporal frequency and finer spatial resolution.

8 Conclusions

Our study provides new information through a wall-to-wall mapping of tropical moist forest cover dynamics over a long-term period (January 1990 to December 2019) at 0.09 ha resolution. This new validated dataset allows to monitor deforestation and degradation in tropical moist forests consistently over a long historical period and at fine spatial resolution. For the first time at the pantropical scale the occurrence and extent of the forest cover degradation is documented on an annual basis in addition to the deforestation. Another innovation consists of characterizing the sequential dynamics of changes by providing transition stages from the initial observation period to the end of the year 2019, i.e. undisturbed forest, degraded forest, forest regrowth, deforested land, conversion to plantations, conversion to water, afforestation, and changes within the mangroves, as well as the timing (dates and duration), recurrence and intensity of each disturbance.

The dynamic maps produced will allow to derive more targeted indicators to measure the achievements in forest, biodiversity, health and climate policy goals from local to international levels (**55**).

Our results should help decision makers on the pressing need to reinforce actions for preserving tropical forest, in particular by avoiding the first scar of degradation that is most likely leading to forest clearance later on.

References

1. Gibson, L., Lee, T. M., Koh, L. P., Brook, B. W., Gardner, T. A., Barlow, J., Peres, C. A., Bradshaw, C. J. A., Laurance, W. F., Lovejoy, T. E., Sodhi, N. S. Primary forests are irreplaceable for sustaining tropical biodiversity. Nature 478, 378–381 (2011). doi:10.1038/nature10425

2. Watson, J. E. M. , Evans, T., Venter, O., Williams, B., Tulloch, A., Stewart, C., Thompson, I., Ray, J. C., Murray, K., Salazar, A., McAlpine, C., Potapov, P., Walston, J., Robinson, ., J. G., Painter, M., Wilkie, D., Filardi, C., Laurance, W. F., Houghton, R. A., Maxwell, S., Grantham, H., Samper, C., Wang, S., Laestadius, L., Runting, R. K., Silva-Chávez, G. A., Ervin, J., Lindenmayer, D. The exceptional value of intact forest ecosystems. Nature Ecology & Evolution 2, 599–610 (2018). Doi:10.1038/s41559-018-0490-x

3. Mackey, B., DellaSala, D. A., Kormos, C., Lindenmayer, D., Kumpel, N., Zimmerman, B., Hugh, S., Young, V., Foley, S., Arsenis, K., Watson, J. E. M. Policy options for the world's primary forests in multilateral environmental agreements. Conserv. Lett. 8, 139–147 (2015). doi:10.1111/conl.12120

4. Luyssaert, S., Schulze, E.-D., Börner, A., Knohl, A., Hessenmöller, D., Law, B. E., Ciais, P., Grace, J. Old-growth forests as global carbon sinks. Nature 455, 213–215 (2008). doi:10.1038/nature07276

5. Aerts, R., Honnay, O. Forest restoration, biodiversity and ecosystem functioning. BMC Ecology, 11, 1-10 (2011). doi:10.1186/1472-6785-11-29

6. Alkama, R., Cescati, A. Biophysical climate impacts of recent changes in global forest cover. Science 351, 600-604 (2016). doi:10.1126/science.aac8083.

7. Grassi, G., House, J., Dentener, F., Federici, S., den Elzen, M., Penman, J. Key role of forests in meeting climate targets but science needed for credible mitigation. Nature Climate Change 7, 220–226 (2017). doi:10.1038/NCLIMATE3227

8. Barlow, J., Lennox, G.D., Ferreira, J., Berenguer, E., Lees, A. C., Mac Nally, R., Thomson, J. R., Frosini de Barros Ferraz, S., Louzada, J., Fonseca Oliveira, V. H., Parry, L., Ribeiro de Castro Solar, R., Vieira, I. C. G., Aragão, L. E. O. C., Anzolin Begotti, R., Braga, R. F., Moreira Cardoso, T., Cosme de Oliveira Jr, R., Souza Jr, C. M., Moura, N. G., Serra Nunes, S., Victor Siqueira, J., Pardini, R., Silveira, J. M., Vaz-de-Mello, F. Z., Carlo Stulpen Veiga, R., Venturier, A., Gardner, T. A. Anthropogenic disturbance in tropical forests can double biodiversity loss from deforestation. Nature 535, 144-147 (2016). doi:10.1038/nature18326

9. Strona, G., Stringer, S. D., Vieilledent, G., Szantoi, Z., Garcia-Ulloa, J., Wich, S., Small room for compromise between oil palm cultivation and primate conservation in Africa. Proc. Natl. Acad. Sci. U.S.A., 115: 8811–8816 (2018). doi: 10.1073/pnas.1804775115

10. Mitchard, E.T.A. The tropical forest carbon cycle and climate change, Nature, 559, 527-534 (2018).

11. Laurance, W. F., Goosem, M., Laurance, S. G. W. Impacts of roads and linear clearings on tropical forests. Trends Ecol. Evol. 24:659–669 (2009). doi:10.1016/j.tree.2009.06.009.

12. Brienen, R., Phillips, O., Feldpausch, T., Gloor, E., Baker, T., Lloyd, J., Lopez-Gonzalez, G., Monteagudo-Mendoza, A., Malhi, Y., Lewis, S. et al., Long-term decline of the Amazon carbon sink Nature, Nature Publishing Group, 519, 344-348, (2015).

13. Baccini, A., Walker, W., Carvalho, L., Farina, M., Sulla-Menashe, D., Houghton, R. A. Tropical forests are a net carbon source based on aboveground measurements of gain and loss. Science 358, 230–234 (2017). doi:10.1126/science.aam5962

14. Brinck, K., Fischer, R., Groeneveld, J., Lehmann, S., Dantas De Paula, M., Pütz, S., Sexton, J. O., Song, D., Huth, A. High resolution analysis of tropical forest fragmentation and its impact on the global carbon cycle. Nat. Commun. 8, 14855 (2017). doi:10.1038/ncomms14855

15. Qie, L. , Lewis, S.L. , Sullivan, M.J.P., Lopez-Gonzalez, G., Pickavance, G.C., Sunderland, T., Ashton, P., Hubau, W., Abu Salim, K., Aiba, S-I., Banin, L.F., Berry,

N., Brearley, F.Q., Burslem, D.F.R.P., Dančák, M., Davies, S.J., Fredriksson, G., Hamer, K.C., Hédl, R., Kho, L.K., Kitayama , K , Krisnawati , H , Lhota , S , Malhi , Y , et al. Long-term carbon sink in Borneo's forests halted by drought and vulnerable to edge effects. Nat. Commun. 8, 1966 (2017) doi: 10.1038/s41467-017-01997-0

16. Pütz, S., Groeneveld, J., Henle, K., Knogge, C., Camargo Martensen, A., Metz, M., Metzger, J. P., Cezar Ribeiro, M., Dantas de Paula, M., Huth, A. Long-term carbon loss in fragmented Neotropical forests. Nature Communications 5, 5037 (2014). doi: 10.1038/ncomms6037

17. Fu, Z., Li, D., Hararuk, O., Schwalm, C., Luo, Y., Yan, L., Niu, S. Recovery time and state change of terrestrial carbon cycle after disturbance. Environ. Res. Lett. 12, 104004 (2017). doi: 10.1088/1748-9326/aa8a5c

18. Olivero, J., Fa, J. E., Real, R., Márquez, A. L., Farfán, M. A., Vargas, J.M. et al. (2017). Recent loss of closed forests is associated with Ebola virus disease outbreaks. Scientific Reports, 7, 14291. https://doi.org/10.1038/s41598-017-14727-9

19. Rulli, M.C., Santini, M., Hayman, D.T.S. and D'Odorico, P. (2017). The nexus between forest fragmentation in Africa and Ebola virus disease outbreaks. Scientific Reports, 7, 41613. https://doi.org/10.1038/srep41613

20. MacDonald, A.J., and Mordecai, E.A., Amazon deforestation drives malaria transmission, and malaria burden reduces forest clearing. PNAS, 116, 22212-22218 (2019). https://doi.org/10.1073/pnas.1905315116

21. Potapov, P., Hansen, M.C., Laestadius, L., Turubanova, S., Yaroshenko, A., Thies, C., Smith, W., Zhuravleva, I., Komarova, A., Minnemeyer, S. et al. The last frontiers of wilderness: Tracking loss of intact forest landscapes from 2000 to 2013. Sci. Adv. 3, (2017). doi: 10.1126/sciadv.1600821

22. Gorelick, N., Hancher, M., Dixon, M., Ilyushchenko, S., Thau, D., Moore, R. Google Earth Engine: Planetary-scale geospatial analysis for everyone. Remote Sens. Environ. 202, 18–27 (2017). Doi: 10.1016/j.rse.2017.06.031

23. Woodcock, C.E. , Allen, R., Anderson, M., Belward, A., Bindschadler, R., Cohen, W., Gao, F., Goward, S.N., Helder, D., Helmer, E., Nemani, R., Oreopoulos, L., Schott, J., Thenkabail, P.S., Vermote, E.F., Vogelmann, J., Wulder, M.A., Wynne, R. Free access to Landsat imagery. Science 320, 1011 (2008). doi: 10.1126/science.320.5879.1011a

24. Hansen, M. C., Potapov, P.V., Moore, R., Hancher, M., Turubanova, S.A., Tyukavina, A., Thau, D., Stehman, S.V., Goetz, S.J., Loveland, T.R. et al. High-resolution global maps of 21st-century forest cover change. Science 342, 850–853 (2013). Doi: 10.1126/science.1244693

25. Kim, D.-H., Sexton, J. O., Noojipady, P., Huang, C., Anand, A., Channan, S., Feng, M., Townshend, J.R. Global, Landsat-based forest-cover change from 1990 to 2000. Remote Sensing of Environment 155, 178-193 (2014). Doi: 10.1016/j.rse.2014.08.017

26. Vancutsem, C., Achard, F., Pekel, J.-F., Vieilledent , G., Carboni, S., Simonetti, D., Gallego, J., Aragao, L., Nasi, R., Long-term (1990-2019) monitoring of tropical moist forests dynamics. Preprint Doi 10.1101/2020.09.17.295774 (submitted to Science Advances).

27. Whitmore, T.C. An introduction to tropical rain forests. Oxford: Clarendon (1990).

28. FAO, Global Ecological Zones for FAO forest reporting: 2010 Update (U.N. Food and Agriculture Organization, 2012). (http://www.fao.org/geonetwork/srv/en/main.home)

29. Wulder, M. A., Masek, J. G., Cohen, W. B., Loveland, T. R., Woodcock, C. E. Opening the archive: How free data has enabled the science and monitoring promise of Landsat. Remote Sens. Environ. 122, 2–10 (2012). doi: 10.1016/j.rse.2012.01.010

30. Markham, B. L., Storey, J. C., Williams, D. L., Irons, J. R. Landsat sensor performance: history and current status. IEEE Transactions on Geoscience and Remote Sensing 42, 2691–2694 (2004).

31. Goward, S., Arvidson, T., Williams, D., Faundeen, J., Irons, J., Franks, S. Historical Record of Landsat Global Coverage Mission Operations, NSLRSDA, and International

Cooperator Stations. Photogrammetric Engineering & Remote Sensing 72, 1155–1169 (2006).

32. Chen, J., Zhu, X., Vogelmann, J.E., Gao, F., Jin, S. A simple and effective method for filling gaps in Landsat ETM+ SLC-off images. Remote Sens. Environ. 115, 1053-1064 (2011). doi:10.1016/j.rse.2010.12.010

33. Pekel, J.-F., Cottam, A., Gorelick, N., Belward, A. S. High-resolution mapping of global surface water and its long-term changes. Nature 540, 418-422 (2016). doi: 10.1038/nature20584

34. Keim, D. A. et al. in Visual Data Mining 76–90, http://kops.uni-konstanz.de/bitstream/handle/123456789/5631/Visual_Analytics_Scope_and_Challenges.pdf?sequence=1&isAllowed=y (Springer, 2008).

35. Yang, J.-B. & Xu, D. L. On the evidential reasoning algorithm for multiple attribute decision analysis under uncertainty. IEEE Trans. Syst. Man Cybern. A 32, 289–304 (2002).

36. Roy, D. P., Ju, J., Kline, K., Scaramuzza, P.L., Kovalskyy, V., Hansen, M. C., Loveland, T.R, Vermote, E., Zhang, C. Web-Enabled Landat Data (WELD): Landsat ETM+ composited Mosaics of the Conterminous United States. Remote Sens. Environ. 114, 35-49 (2010). doi:10.1016/j.rse.2009.08.011

37. Potapov, P. V., Turubanova, S. A., Hansen, M. C., Adusei, B., Broich, M., Altstatt, A., Mane, L., Justice, C.O. Quantifying forest cover loss in Democratic Republic of the Congo, 2000– 2010, with Landsat ETM+ data. Remote Sens. Environ. 122, 106-116 (2012) doi:10.1016/j.rse.2011.08.027

38. Margono, A., Turubanova, S., Zhuravleva, I., Potapov, P., Tyukavina, A., Baccini, A., Goetz, S., Hansen, M. C. Mapping and monitoring deforestation and forest degradation in Sumatra (Indonesia) using Landsat time series data sets from 1990 to 2010. Environmental Research Letters 7, 034010 (2012). doi:10.1088/1748-9326/7/3/034010

39. Griffiths, P., Kuemmerle, T., Baumann, M., Radeloff, V.C., Abrudan, I.V., Lieskovsky, J., Munteaunu, C., Ostapowicz, K., Hostert, P. Forest disturbances, forest recovery, and changes in forest types across the Carpathian ecoregion from 1985 to 2010 based on Landsat Image Composites. Remote Sens. Environ. 151, 72-88 (2014). doi:101016/j.rse.2013.04.022

40. Potapov, P. V., Turubanova, S. A., Tyukavina, A., Krylov, A. M., McCarty, J. L., Radeloff, V. C., Hansen, M. C. Eastern Europe's forest cover dynamics from 1985 to 2012 quantified from the full Landsat archive. Remote Sens. Environ. 159, 28-43 (2015). doi:10.1016/j.rse.2014.11.027

41. Muller, H., Griffiths, P., Hostert, P. Long-term deforestation dynamics in the Brazilian Amazon - Uncovering historic frontier development along the Cuiabá–Santarém highway. International Journal of Applied Earth Observation and Geoinformation 44, 61-69 (2016). doi: 10.1016/j.jag.2015.07.005

42. Hermosilla, T., Wulder, M. A., White, J.C., Coops, N .C.,, Hobard, G. W. Updating Landsat time series of surface-reflectance composites and forest change products with new observations. International Journal of Applied Earth Observation and Geoinformation 63, 104-111 (2017). doi: 10.1016/j.jag.2017.07.013

43. Smith, A. R. Color gamut transform pairs. Comput. Graph. 12, 12–19 (1978).

44. Sanderson, E. W., Jaiteh, M., Levy, M. A., Redford, K. H., Wannebo, A. V., Woolmer, G. The human footprint and the last of the wild. Bioscience 52, 891–904 (2002). Doi:10.1641/0006-3568(2002)052

45. Thompson, I., M.R, Okabe, K., Bahamondez, C., Nasi, Heymell, R., Sabogal S., An Operational Framework for Defining and Monitoring Forest Degradation. Ecology and Society 18(2):20 (2013). doi: 10.5751/ES-05443-180220

46. Congalton, R.G., Green, K. Assessing the accuracy of remotely sensed data: principles and practices. Lewis publishers. 137 pp. (1999)

47. Stehman, S. V. Sampling designs for accuracy assessment of land cover. International Journal of Remote Sensing 30, 5243-5272 (2009). doi:10.1080/01431160903131000

48. Defourny, P., Schouten, L., Bartalev, S., Bontemps, S., Caccetta, P., de Wit, A.J.W., Di Bella, C., Gérard, B., Giri, C., Gond, V., Hazeu, G.W., Heinimann, A., Herold, M., Knoops, J., Jaffrain, G., Latifovic, R., Lin, H., Mayaux, P., Mücher, C.A., Nonguierma, A., Stibig, HJ., Van Bogaert, E., Vancutsem, C., Bicheron, P., Leroy, M., Arino, O. Accuracy Assessment of a 300 m Global Land Cover Map: The GlobCover Experience. In 33rd International Symposium on Remote Sensing of Environment, Sustaining the Millennium Development Goals. pp. 1–5, (2009).
49. Wolter, K. M. An investigation of some estimators of variance for systematic sampling. Journal of the American Statistical Association 79, 781-790 (1984).
50. Gallego, F. J., Delincé, J. The European Land Use and Cover Area-frame statistical Survey (LUCAS), in Agricultural Survey Methods, ed: R. Benedetti, M. Bee, G. Espa, F. Piersimoni, Ch. 10. pp. 151-168, John Wiley & sons (2010).
51. Benedetti, R., Piersimoni, F., Postiglione, P. Sampling spatial units for agricultural surveys, Springer. Berlin (2015).
52. Cochran, W. G. Sampling techniques (3rd ed.). New York: John Wiley & Sons (1977).
53. Olofsson, P., Foody, G. M., Herold, M., Stehman, S. V., Woodcock, C. E., Wulder, M.A. Good practices for estimating area and assessing accuracy of land change. Remote Sens. Environ. 148, 42–57 (2014).
54. Corbane, C., Politis, P., Kempeneers, P., Simonetti, D., Soille, P., Burger, A., Pesaresi, M., Sabo, F., Syrris, V. & Kemper, T. (2020). A global cloud free pixel-based image composite from Sentinel-2 data. Data in Brief, 105737.
55. Finer, M., Novoa, S., Weisse, M. J., Petersen, R., Mascaro, J., Souto, T., Stearns, F., García Martinez R., Combating deforestation: From satellite to intervention. Science 360, 1303-1305 (2018). doi:10.1126/science.aat1203.
56. Petersen, R., Aksenov, D., Esipova, E., Goldman, E., Harris, N., Kuksina, N., Kurakina, I., Loboda, T., Manisha, A., Sargent, S., Shevade, V. Mapping tree plantations with multispectral imagery: preliminary results for seven tropical countries. Technical Note, Washington, DC: World Resources Institute (2016).
57. Harris, N., E. Goldman and S. Gibbes. Spatial Database of Planted Trees (SDPT) Version 1.0., Technical Note, Washington, DC: World Resources Institute (2019).
58. Vijay, V., Pimm, S. L., Jankins, C. N., Smith, S. J. The impacts of Oil Palm on Recent Deforestation and biodiveristy Loss. PLOS ONE 11, e01599668 (2016). doi: 10.1371/journal.pone.0159668Congalton, R.G., Green, K. Assessing the accuracy of remotely sensed data: principles and practices. Lewis publishers. 137 pp. (1999).
59. Bunting, P., Rosenqvist, A., M. Lucas, R., Rebelo, R.M., Hilarides, L., Thomas, N., Hardy, A., Itoh, A., Shimada M., and Finlayson, C.M., The Global Mangrove Watch - A New 2010 Global Baseline of Mangrove Extent. Remote Sens. 10 (2018).
60. Eva, H.D., de Miranda, E.E., Di Bella, C.M., Gond, V., Sgrenzaroli, M., Jones, S., Countinho, A., Dorado, A., Guimaraes, M., Achard, F., Belward, A.S., Barholome, E., Baraldi, A., De Grandi, G., Vogt, P., Fritz, S., Hartley, A., A vegetation map of South America. European Commission report 20159 EN (2002).
61. Killeen, T.J., Jardim, A., Mamani, F., Rojas, N. Diversity, composition and structure of a tropical semideciduous forest in the Chiquitanía region of Santa Cruz, Bolivia. Journal of Tropical Ecology 14 (1998).

List of abbreviations and definitions

ENSO   El Niño southern oscillation

ETM+   Enhanced Thematic Mapper-plus

GFC   Global Forest Change

GLC2000   Global Land Cover 2000

HR   High-resolution

HSV   hue, saturation, value

NDCs   Nationally Determined contributions

NDWI   Normalized Difference Water Index

NIR   near infrared

OLI   Operational Land Imager

SDGs   Sustainable Development Goals

TM   Thematic Mapper

TMF   Tropical Moist Forest

USGS   US Geological Survey

SLC   scan line corrector

SWIR   short-wave infrared

TIR   thermal infrared band

List of figures

60

List of tables

Annexes

Annex 1. Ancillary data

Three ancillary datasets were used to spatially attribute disturbances (i) to the conversion to commodities or tree plantations (mainly oil palm and rubber), (ii) to the conversion to water bodies (conversion mainly due to new dams), and (iii) to specific changes within the mangroves.

1. Conversion to commodities or tree plantations

In the transition map, commodities (oil palm) or tree plantations (rubber) appear either as deforested land or other land cover class when established during the monitoring period or before the initial period respectively. They can also appear as undisturbed forest or forest regrowth when established a long time before the initial period with a spectral signature similar to a forest or a forest regrowth, e.g. in the case of old oil palm plantations.

In order to reduce these commission errors we created a mask of commodities or tree plantations from two external data sources: (i) the planted tree datasets from the World Resources Institute (WRI) (**56-57),** which cover 14 countries (Brazil, Cambodia, Colombia, Indonesia, Liberia, Malaysia, Peru, Chili, Gabon, Ghana, Argentina, Honduras, Guatemala, Australia) and several plantation types, from which we only used 'Large industrial plantations' and 'Clearing/very young plantation not mosaic', and (ii) the oil palm dataset from Duke University (**58**), which covers a few plantation zones in the tropics.

Both datasets have been checked visually against high-resolution (HR) images available from Google Earth Engine (GEE) (**22**) and areas that are validated by the photo-interpreter as covered by commodities and with a correct delineation are incorporated in the commodities mask. Commodities that are well identified on the HR images but with a wrong delineation have been manually re-delineated by the interpreter and incorporated in the commodities mask.

Then we carried out a further control of the transition map to identify and delineate missing areas of commodities that are not identified from existing databases. This step was done through a systematic analysis within the transition map for all areas with specific geometric shapes corresponding to plantations. These commodities were delineated visually by the photo-interpreter and incorporated in the commodities mask.

This new class of commodities allows also assessing the area of conversion of moist forests to such commodities. All pixels of the commodities mask are reassigned to the classes of conversion to commodities, e.g. a pixel that was initially labelled as deforested is reclassified as "conversion to commodities" with three sub-classes: establishment before 2000, in 2000-2009, in 2010-2019.

2. Conversion to water

To identify conversion from moist forests to water bodies, which are usually due to the creation of a dam, we used the Global Surface Water (GSW) dataset derived from Landsat time series over the period 1984-2015 (**33**) and the GSW updates for the period 2016-2019. This allowed to create two additional classes of deforestation: (i) forest conversion to a permanent water body and (ii) forest conversion to a seasonal water body. The GSW time series also provided information on the start date of forest conversion (flooding) when the forest was directly flooded without prior clearance. We have also integrated the inter-annual variations of the water bodies in our annual change product by discriminating permanent water from seasonal water from other land cover classes.

3. Changes within the mangroves

We created a specific class of mangroves to assess the status and changes of this specific forest ecosystem. We used the Global Mangrove Watch (GMW) dataset (**59**) to create an initial map of mangroves. As the GMW dataset covers the years 1996 and 2006, we first produced a maximum extent mask of the mangroves during the period 1996-2006 and then reassigned the transition classes under the maximum extent mask to produce a map of changes in mangroves. As example of reassignment, "undisturbed TMF (class 10 of the transition map)" is reclassified as "undisturbed mangrove (class 12)". Eight classes of changes within the mangroves (including degradation, regrowth and deforestation) have been documented with sub-classes for each period of disturbance.

Annex 2. Specific tropical forest types

(i) The tropical moist forest areas with bamboo dominance might be mis-classified as disturbed forests due seasonal or occasional defoliation of the bamboos. Therefore, we use a specific approach to map (as a specific class 11 of the transition map) the bamboo-dominated forests (*pacales*) in two specific zones where they are present over large areas: the Brazilian state of Acre and of east Peru. We first created a spatial mask for reclassifying false disturbances in these two zones. The spatial mask is created from the South-America regional part of the Global Land Cover 2000 (GLC2000) map (**60**) combined with a visual interpretation of recent high-resolution imagery. Dedicated decision rules are then applied for pixels classified as disturbed forest cover within this mask based on the recurrence, intensity and distance from roads and rivers of the disruption events to separate false disturbances from real disturbances (e.g. disturbances within 120 m from roads are kept).

(ii) Our tropical moist forest domain includes semi-deciduous forests that appear as evergreen forests along a full year. However, specific types of forest transitions between the humid and dry ecosystem domains, e.g. the Chiquitania forests of northern Bolivia (**60-61**) can behave alternatively as evergreen or seasonal forests during specific years depending on the yearly amount and distribution of precipitations (**61**). If these forests behave as evergreen at the beginning of the Landsat archive, temporary defoliation due to drier conditions in the second part of the archive may be mis-classified as a disturbance, e.g. as a degradation when defoliation is observed along less than a duration of 900 days. We apply here also dedicated classification rules for avoiding such misclassifications due to the variable seasonal character of this specific forest type. The rules are based on the recurrence and intensity of the disruption events and are combined with a spatial mask that is created from the South-America regional component of the GLC2000 map (**60**) and visual interpretation of high-resolution imagery.

(iii) Some savanna wetlands (wet meadows or marshes) can be misclassified as forest or disturbed forests due the scarcity of dryness periods. Such errors are expected to be limited due to (i) the consideration of a minimum duration for the initial period and (ii) the use of the GWSE dataset that documents the water seasonality. A region that is regularly flooded since the beginning of the observation period is assigned to the permanent or seasonal water class and hence cannot be classified as a TMF. However, for regions with geographic and temporal discontinuities in the Landsat archive occasionally or never detected as water, and/or with gaps caused by persistent cloud cover, periods of dryness may be not well covered with Landsat imagery during the initial reference period. To avoid these commission errors, wetlands areas have been identified using the Global Wetland atlas (https://www2.cifor.org/global-wetlands/) and the GLC 2000 map (**60**), with a further visually check on HR imagery. When misclassification was detected, these areas have been visually delineated and re-assigned to the 'other land cover' class (# 90 in the transition map).

Annex 3. Legend of the Transition map

- 10. Undisturbed tropical forest (1982-2019)
- 11. Bamboo dominated forest
- 12. Undisturbed mangroves (1982-2019)
- 20. Degraded forest before the observation period
- 21. Degraded forest with short-duration disturbance (before 2000)
- 22. Degraded forest with short-duration disturbance (in 2000-2009)
- 23. Degraded forest with short-duration disturbance (in 2010-2018)
- 24. Degraded forest with long-duration disturbance (before 2000)
- 25. Degraded forest with long-duration disturbance (in 2000-2009)
- 26. Degraded forest with long-duration disturbance (in 2010-2018)
- 27. Degraded forest with 2/3 short degradation periods (before 2000)
- 28. Degraded forest with 2/3 short degradation periods (in 2000-2009)
- 29. Degraded forest with 2/3 short degradation periods (in 2010-2019)
- 31. Old regrowth (more than 20 years)
- 32. Young regrowth (between 10 and 20 years)
- 33. Very young regrowth (between 3 and 10 years)
- 40. Deforestation started before 2000
- 41. Deforestation started in 2000-2009
- 42. Deforestation started in 2010
- 43. Deforestation started in 2011
- 44. Deforestation started in 2012
- 45. Deforestation started in 2013
- 46. Deforestation started in 2014
- 47. Deforestation started in 2015
- 48. Deforestation started in 2016
- 51. Deforestation started in 2017 *
- 52. Deforestation started in 2018 *
- 53. Deforestation started in 2019 *
- 54. Degradation started in 2019 *
- 61. Degraded Mangroves (before 2010)
- 62. Degraded Mangroves (in 2010-2018)
- 63. Mangrove regrowthing (more than 10 years)
- 64. Mangrove regrowthing (between 3 and 10 years)
- 65. Mangrove deforested (started before 2000)
- 66. Mangrove deforested (started in 2000-2009)
- 67. Mangrove deforested (started in 2010-2016)
- 68. Mangrove recently disturbed (started in 2017-2019)
- 71. Permanent Water
- 72. Sesaonal Water
- 73. Deforestation to Permanent Water
- 74. Deforestation to Seasonal Water
- 81. Old Plantations (deforested before 1990)
- 82. Plantation regrowthing (deforested before 2010)
- 83. Plantation regrowthing (deforested in 2010-2016)
- 84. Deforestation in the plantation started before 2000
- 85. Deforestation in the plantation started in (2000-2009)
- 86. Deforestation in the plantation started in (2010-2016)
- 87. Recent disturbance(s) in the plantation (2017-2019)
- 91. Other LC
- 92. Other LC recently regrowthing (between 3 and 10 years)
- 93. Other LC regrowthing (between 10 and 20 years)
- 94. Other LC: From water to Regrowth

Annex 4. Legend of the Annual change maps

- 1. Tropical moist forest
- 2. Tropical moist forest later converted in plantation
- 3. New degradation
- 4. Ongoing degradation
- 5. Degraded forest
- 6. New deforestation
- 7. Ongoing deforestation
- 8. New regrowth
- 9. Regrowthing
- 10. Other land cover (not water)
- 11. Permanent Water
- 12. Seasonal Water
- 13. Nodata - TMF domain
- 14. Initial period with at least 1 valid obs - TMF domain
- 15. Nodata - Other LC or TMF converted

The European Commission's science and knowledge service

Joint Research Centre

JRC Mission

As the science and knowledge service of the European Commission, the Joint Research Centre's mission is to support EU policies with independent evidence throughout the whole policy cycle.

EU Science Hub

ec.europa.eu/jrc

@EU_ScienceHub

EU Science Hub - Joint Research Centre

EU Science, Research and Innovation

EU Science Hub

Publications Office
of the European Union